Interaction Between Oxidation and Stress at High Temperatures on Scale Growth of Fe-Cr-Al Based Alloy

Somaradi Khiev

INTERACTION BETWEEN OXIDATION AND STRESS AT HIGH TEMPERATURES ON SCALE GROWTH OF Fe-Cr-Al BASED ALLOY

By

SOMARADI KHIEV, B. APP. SC.

A Thesis
Submitted to the School of Graduate Studies
in Partial Fulfilment of the Requirements
for the Degree
Master of Applied Science

McMaster University

MASTER of APPLIED SCIENCE (2009) McMaster University
(Department of Materials Science and Engineering) Hamilton, Ontario

TITLE: Interaction Between Oxidation and Stress at High Temperatures on Scale Growth of Fe-Cr-Al Based Alloy

AUTHOR: Somaradi Khiev, B. App. Sc. (University of Windsor)

SUPERVISOR: Dr. D. S. Wilkinson

NUMBER OF PAGES: xiv, 80

Abstract

The need for environmentally friendly and energy efficient high temperature components that can operate under mechanical and/or thermal stress has prompted interest in the development of Fe-Cr-Al based alloys. These alloys have been widely investigated, because of their ability to form a protective layer of $\alpha - Al_2O_3$, which is able to withstand further oxidation degradation. However, despite their superior oxidation qualities, alpha-alumina scales are highly susceptible to mechanical damage when subjected to aggressive environments. The origins of such failure can be attributed to the generation and relaxation of stresses during the scaling process. As such, this study has experimentally investigated the interaction between oxidation and stress on Fe-Cr-Al based alloy, Kanthal Al.

Oxidation experiments of Kanthal Al were conducted in two parts. First, the alloy's scaling process at rest with respect to intrinsic growth stress and oxide morphology was examined. Second, external stress was applied during oxidation to obtain a comprehensive understanding of its effect on scale growth with comparison to experiments conducted without stress.

The formation of compact $\alpha - Al_2O_3$ scales was accompanied by compressive growth stresses on the order of 1 GPa. Prolonged oxidation decreased growth stresses resulting in increased scale porosity. Maximum scale porosity occurred under oxidation at 1300°C. Consequently, the protectiveness of the scale was heavily degraded, as indicated by scale morphology, implying that in-service operation at this temperature or above would be detrimental.

Applied tensile stress showed a significant decrease in the development of intrinsic growth stress, suggesting a strong interdependency between scale growth stress and creep deformation at high temperature. There was no measurable change in the scale growth rate, as compared to experiments conducted at rest. Possible explanations include insufficient tensile load and/or drastic increase in spallation/rehealing, both of which simultaneously influences the lifetime of a material under aggressive operational conditions.

Acknowledgments

When I asked what is the key to a successful Master Degree of Applied Science, many answer: determination, confidence, intelligence, etc. I now know there is more to the story.

Key to a Successful Graduate Degree: A Company of Great People

First, you want a patient supervisor who gives you the freedom to learn and grow, by allowing you to make mistakes; because, there will be many, and many will be costly. Without their patience and understanding your project will not end well. Sorry Dr. Wilkinson for breaking so many things.

Second, on the days where you wake up and say, "that's it, I'm quitting". Make certain you have a friend to remind you that no task is impossible, and has the ability to somehow give you confidence, especially where there is none. And if all else fails, make sure they drink. Because only alcoholics drink by themselves, and social butterflies drink with friends. Here's to you Grand Master Shery.

Next, you will have to present your work, this will be no pleasant task. To overcome this, the recipe calls for: 1 part fear, 1 part interesting slides that last 35 minutes, and 8 parts drive from a good friend who only wants to see you succeed. I think Daisy was more nervous than I was.

When you run experiments you might find that cereal is your best friend. When this happens, be sure to have a friend that likes cooking, and is generous enough to feed you. Thanks Ana for feeding me for at least a year!

Now, to get any meaningful data you will have to analyze your specimens. Sometimes, this process can be very tiresome. For me, it was like watching paint dry. If this is also the case for you, make sure that whomever you're with is full of gossip, laughter and spirit. It will make the time flies by. Julias are good for this.

Usually, sample analysis means large amounts of data that must be complied. The best is to use MATLAB. At first it may seem overwhelming, but if you have a good Manuel you will have no problem. They are full of useful information, and are always available to help. Oh sorry, the term is handbook not Manuel.

Next, is the all so dreaded task of writing your thesis. This part, pay very close attention, it's the most important. Ensure to have a little Asian by your side abusing and motivating you to work. Because when this time rolls around, you will only want to sleep. These little Asians are like drill sergeants, they love yelling and poking you with their needlelike fingers. It definitely keeps you working. I can still hear the words echoing from my little Asian, "sleep is luxury you cannot afford". Ah, sweet memories! That reminds me, we should play squash again Lina.

Lastly, and most importantly, have a great family. The kind that indulges your ridiculous spending habits, just because they know it makes you happy. But, mostly the kind that always has faith, supports your every decision, and will always be there for through the thick of it. Thank you so much Mom and Sis. Love you.

I would like to extend a very special thanks to Andi Limarga, who tirelessly performed PSLS on all my specimens and answer every single question I had, even if it took up an entire afternoon. This work would not be possible without his help. David R. Clarke, Andi's supervisor who was kind enough to spare Andi for months in order to help. Jim Garret for his creativity.

Thank you to all who have made this experience unforgettable. You know who you are.

Yours truly,

Somaradi

Contents

List of Figures

List of Tables

Chapter 1

Introduction

The need for environmentally friendly and energy efficient components used primarily for high temperature applications has created a growing interest in the development of Iron-Chromium-Aluminium (Fe-Cr-Al) based alloys for industrial service above 1100°C (Wilber et al., 2000; Badini and Laurella, 2001; Jedlinski, 1997). This interest is derived from the material's ability to form a homogeneous protective scale, alpha-alumina, capable of preventing further oxidation degradation (Berthome et al., 2005; Badini and Laurella, 2001; Blachčre et al., 2003; Stott, 1997). Unfortunately, despite their outstanding performance, alpha-alumina scales are still very susceptible to mechanical damage, i.e. cracking, spallation and creep deformation of the metal and the oxide when subjected to aggressive environments: thermal cycling, mechanical stress and high temperatures (Jedlinski, 1997; Cueff et al., 2003). The origins of these failures, among other factors, can be attributed to the relaxation of stresses. These stresses are generated during the scaling process, namely oxide formation and thermal expansion mismatch between the oxide and the substrate, the latter being more significant. As such, most researchers have focused their studies on improving the performance of Fe-Cr-Al alloys by understanding the growth and life of Al_2O_3

scales at high temperatures.

The interaction between stress generation, namely growth stress, and stress relaxation, namely creep deformation, has been of interest for many years. The existence of the individual effects has been published in papers dating back as early as 1923 by Pilling and Bedworth, pioneers in this field of study (Rhines and Wolf, 1970). However, there is limited research on the combined effects. Recently, investigations involving creep effects on the oxidation characteristics of Fe-Si alloys (Rolls and Shahhosseini, 1982), and oxidation of Ni-20Cr alloys subjected to a mechanical load (Calvarin-Amiri et al., 2000, 2001) have suggested that the application of a tensile force during oxidation would allow for continual growth of the oxide scales, by aiding lateral expansion of the substrate and mechanically relieving growth stresses. Such findings inferred that scale thickening is inhibited by compressive stresses induced through the impediment of lateral expansion of the substrate.

In order to further understand the development of growth stresses the above theory was recently revisited through numerical modeling using $\gamma - TiAl$ class alloys under bending loads (Limarga and Wilkinson, 2006). Although this modeling work generated good agreement with the work of earlier predecessors (Tolpygo and Clarke, 1998a), experimental results on oxidation and nitriding of $\gamma - TiAl$ posed difficulties for conclusive model validation. Firstly, oxidation experiments were unfavorable in that they produced porous, complex and fast growing oxides that were easily spalled. Secondly, despite preliminary results with nitridation experiments, the formed scale system was still far too complex for thorough analysis required for obtaining parameters as input for the corresponding numerical model. The reason is that the nitrides were multilayered, and upon continual nitridation, a titanium deficiency occurred resulting in the formation of unwanted titanium aluminides. As such a simpler metal/oxide system was chosen for this present study to better understand the relationship between stress generation, stress relaxation and external stress, experimentally.

For this study an 'alumina forming' iron-chromium-aluminum based alloy, known as Kanthal A1, was selected. This material was chosen based on its ability to form a simple single layered protective oxide, alpha-alumina, which has good creep resistance. Additionally, the metal/scale system allows for concurrent diffusion of both oxygen and aluminum, indicated by formation of both columnar and equiaxed oxide grains, enabling the development of compressive intrinsic growth stress on the order of 1 GPa at temperatures above 1200°C, which is required for the formation of pure alpha-alumina scales.

The study will start with a basic background on the generation and relaxation of oxide compressive stresses, discussed in two separate chapters, Chapters 2 and 3 respectively. Due to the complex nature of the oxidation process only specific topics directly related to this work will be reviewed in detail in these chapters. Experimental procedures including characterization techniques are elaborated in Chapter 4. Next, experimental results will be discussed in detail in Chapter 5. A general outline is listed below.

- Confirmation of the crystallographic nature of the formed scale
- General examination of scale cross-sectional microstructure under oxidation conditions
- Thorough comparative investigation of the competition between stress generation and relaxation on scale thickness and microstructure with and without load as a function of time and temperature
    - Cross-sectional display of the microstructural evolution

  - Quantitative determination of oxide thickness
  - Measurement of residual stress at room temperature
  - Calculation of intrinsic growth stress derived from corresponding residual stress values

Lastly, the culmination of this work will be summarized in the final chapter. It will highlight the significance of this work with respect to earlier investigations in the related field, that the application of a tensile stress reduces the accumulation of compressive stresses developed during scale growth in an oxidizing environment. Additionally, future suggestions corresponding to this study will be provided.

Chapter 2

Generation of Compressive Stresses During Scale Formation

The existence of compressive stresses generated from high-temperature oxidation of alumina-forming alloys has been known for many years . They have been confirmed by x-ray diffraction and recently photo-luminescence piezo-spectroscopy (PSLS) (Lipkin and Clarke, 1996; Clarke et al., 2004). However, their origin and the impact they have on the mechanical integrity of a scale is still subject to much debate (Clarke, 2003). This chapter will discuss the development of two stress contributors, namely thermal expansion mismatch and intrinsic growth stress.

2.1 Thermal Expansion Mismatch

In general, exposure of a substrate and adherent scale to high temperatures will create a compressive stress within the scale upon cooling. The development of the thermal stress due to cooling is illustrated in Figure 2.1.

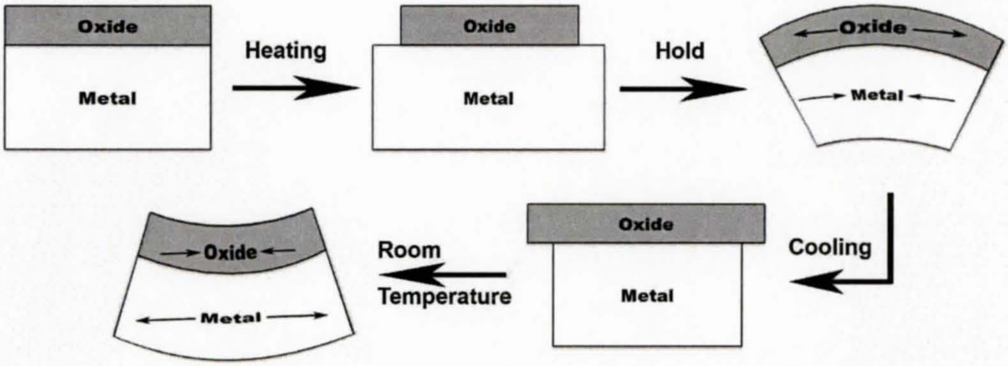

Figure 2.1. Schematic illustration of compressive development due to thermal expansion mismatch between oxide and metal (Limarga and Wilkinson, 2006)

The illustration in Figure 2.1 explains that a mismatch in thermal expansion coefficients will force the substrate to expand at a faster rate than that of the scale. However, since the substrate is constrained by the scale, the rate of substrate expansion will be restricted to the rate of scale expansion. This will create a compressive stress in the metal and tensile stress in the scale during high temperature exposure, as dictated by mechanical equilibrium. Upon cooling the substrate will contract faster than the scale. Again, the scale restricts the substrate from contraction, resulting in the reverse effect, i.e. tensile stresses in the metal and compressive stresses in the scale

Stresses in the scale due to thermal expansion mismatch are formulated in Equation 2.1 (Tolpygo and Clarke, 1998a), where E is the Young's modulus, ν Poisson's ratio, α coefficient of thermal expansion, h thickness, ΔT is temperature difference upon cooling ($T_{final} - T_{initial}$), and subscripts ox and m represent oxide and metal, respectively. If the scale is much thinner than the substrate, i.e. the ratio of h_{ox}/h_m is small, say less than 0.1% ($h_{ox}/h_m \rightarrow 0$), then Equation 2.1 reduces to Equation 2.2 (Tolpygo and Clarke, 1998b). In this study, Equation 2.2 will be used for all calculation purposes. Basic property values and calculated thermal stresses are listed in Table 2.1. Note that the mismatch between thermal expansion coefficients can generate a compressive stress on the order of 3 - 4 GPa.

$$\sigma_{ox}^{T} = \frac{E_{ox}(\alpha_{ox} - \alpha_m)\Delta T}{(1 - \nu_{ox}) + \frac{h_{ox}}{h_m}\frac{E_{ox}}{E_m}(1 - \nu_m)} \tag{2.1}$$

$$\sigma_{ox}^{T} \approx \frac{E_{ox}(\alpha_{ox} - \alpha_m)\Delta T}{(1 - \nu_{ox})} \tag{2.2}$$

Table 2.1: Properties used for calculations of thermal stresses due to cooling. Values were calculated using Equation 2.2 (Tolpygo and Clarke, 1998a).

Temperature (^{o}C)	Thermal Expansion Coefficient (^{o}C^{-1})		Young's Modulus (GPa)		Poisson Ratio		Thermal Stress (GPa)
	$\alpha_{ox} \cdot 10^{-6}$	$\alpha_m \cdot 10^{-6}$	E_{ox}	E_m	ν_{ox}	ν_m	σ_{ox}^T
25			400	190	0.25	0.3	
1000	8.5	14.3	350	-	-	-	-3.02
1100	8.6	14.6	340	-	-	-	-3.44
1200	8.7	14.9	330	-	-	-	-3.89
1250	8.75	15.0	325	-	-	-	-4.08
1300	8.8	15.1	320	-	-	-	-4.28

2.2 Intrinsic Growth Stress

The earliest investigation that recognized the importance of oxidation related growth stress was conducted by Pilling and Bedworth in 1923 (see Rhines and Wolf, 1970). They postulated that the generation of stress during oxide formation was a result of a volume dilatation upon the conversion of a metal to its oxide, defined as the Pilling-Bedworth Ratio (PBR), Φ:

$$\Phi = \frac{\Omega_{ox}}{\Omega_m} \tag{2.3}$$

where Ω_{ox} and Ω_m are the volume per metal ion in the oxide and volume per metal atom in the metallic phase, respectively (Pilling and Bedworth, 1923).

The PBR predicts the protectiveness of an oxide and the sign and magnitude of its growth stress. If the oxide is compact or continuous in structure, PBR will be greater than 1. However, if the opposite is true, the ratio will be less than 1. Based on these observations, Pilling and Bedworth concluded that the generation of a compressive oxide growth stress favored the formation of protective compact oxide by reducing the permeability of oxygen through the film. In contrast, oxides with tensile growth stresses would result in a porous structure, which provides no impedance to further oxidation as continual penetration of oxygen is allowed (Pilling and Bedworth, 1923). Summary of their findings is shown in Table 2.2, and note that Al_2O_3 has a PBR greater than 1 indicating that the scale will be compact and its growth stress will be compressive.

Table 2.2: Pilling and Bedworth Ratios for various oxides (Pilling and Bedworth, 1923).

Oxide	MgO	$\mathbf{Al_2O_3}$	CuO	NiO	FeO	TiO_2
Φ	0.81	**1.28**	1.64	1.65	1.70	1.73

Years later Rhines and Wolf (1970) established a powerful idea that profoundly impacted the direction of research in high temperature oxidation. They suggested that the development of stresses from scale growth was due to a counter concurrent flux of metal and oxygen ions. Both fluxes meet at the grain boundary network of the pre-existing scale that lies perpendicular to the metal substrate, which allows for the deposition of new oxides, shown schematically in Figure 2.2. Growth of the newly deposited oxides results in lateral expansion of the scale at the grain boundary. However, the lateral expansion of the scale is restrained by the underlying metal substrate. Consequently, the scale is unable to extend and provide additional space required for insertion of new oxides, which develops a compressive stress in the oxide. Microscopic evidence of their findings is shown in Figure 2.3.

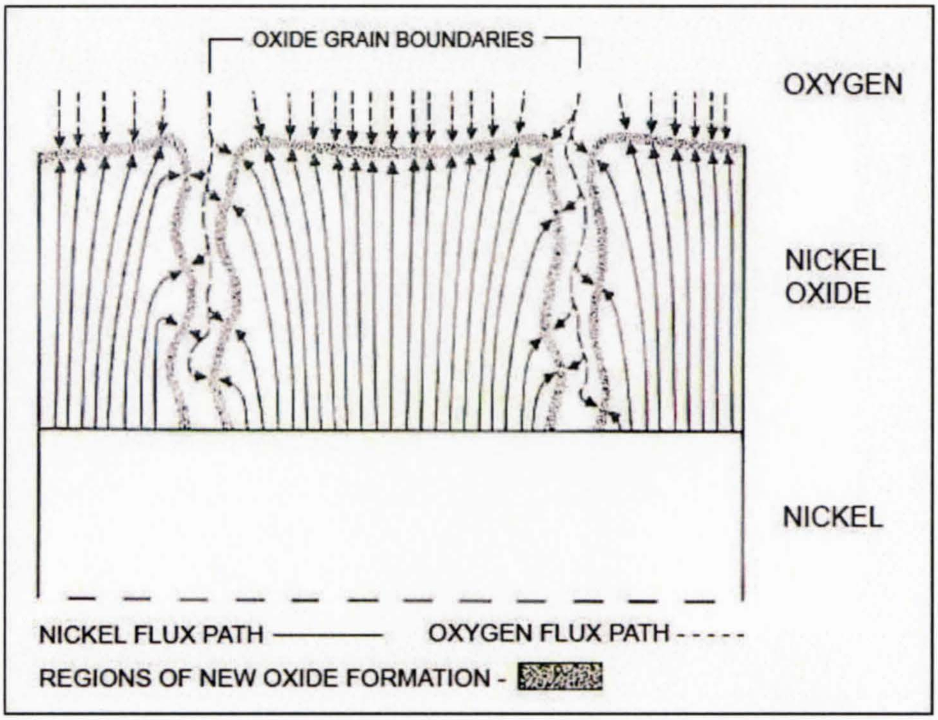

Figure 2.2: Schematic of flux of nickel and oxygen through the grain boundary network (Rhines and Wolf, 1970).

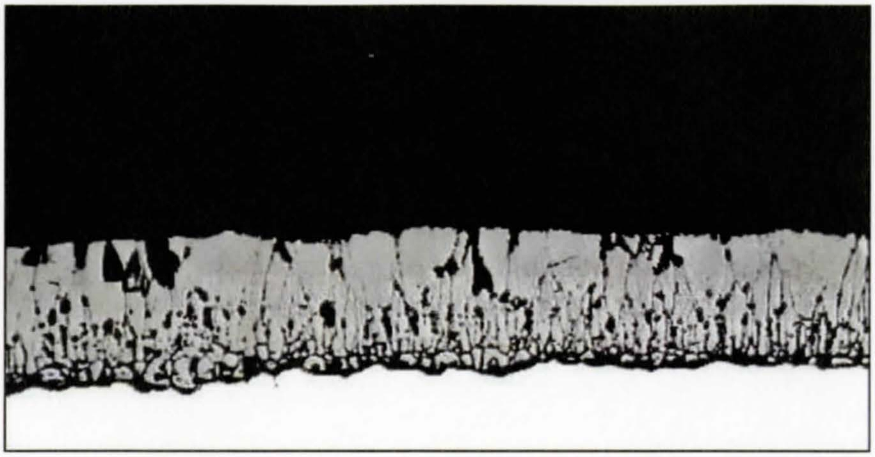

Figure 2.3: SEM micrograph of NiO showing undergrowth of NiO at the metal/oxide interface (Rhines and Wolf, 1970)

To date, there have been several investigations following Rhines and Wolf's model: inward diffusion of oxygen ions and outward diffusion of metal ions, meeting at the pre-existing grain boundary network of the scale. One particular investigation was a two-stage 'wedge' oxidation experiment (Figure 2.4) (Tolpygo and Clarke, 2003; Nychka and Clarke, 2005) In this work a pre-oxidized substrate was polished to remove the porous top layer of the oxide, leaving behind the columnar grains. Such a sample was then re-oxidized in order to observe the behavior of new oxide growth. After re-oxidation the grain boundaries of the pre-existing scale was decorated with new oxides. Presence and location of these new oxides suggested an outward diffusion of cations (Al^{3+}) along the underlying grain boundaries Figure 2.5. Additionally, continued scale growth at the metal/oxide interface was observed with no morphology change, thus indicating concurrent flux of oxygen into the system.

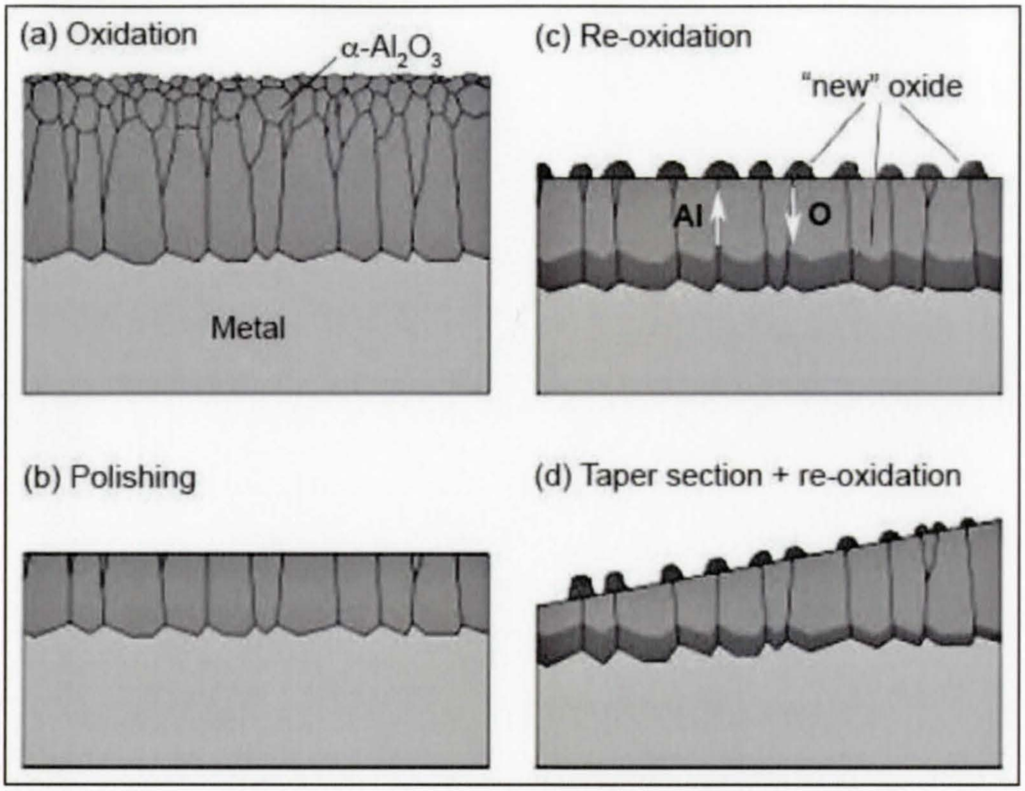

Figure 2.4: Schematic of two-stage oxidation wedge experiment (Tolpygo and Clarke, 2003).

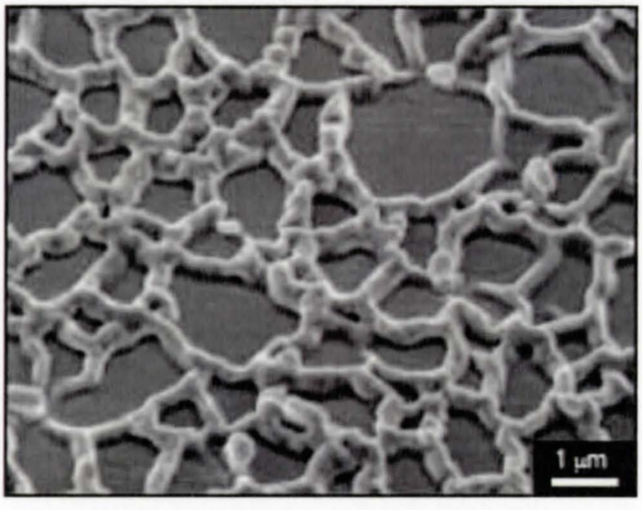

Figure 2.5: SEM micrograph of Al_2O_3 scale growing along the grain boundaries after re-oxidation (Tolpygo and Clarke, 2003).

In addition to the decoration of grain boundaries with oxides, the fractured cross-section of the scale shown in Figure 2.6 indicates three noteworthy characteristics: (1) the inner scale (metal/oxide interface) is columnar and the outer portion (oxide/gas interface) is equiaxed, (2) there is no crystallographic texture indicating the grains are randomly oriented despite the columnar microstructure, and (3) the scale/metal interface is faceted with the imprint of individual alumina grains. The presence of two distinct scale structures suggests two diffusing species within the scale (Al^{3+} and O^{2-}) It is believed that the columnar structure is a consequence of inward diffusion of oxygen, and the equiaxed layer is attributed to outward diffusion of aluminum along the grain boundaries (Clarke, 2003)

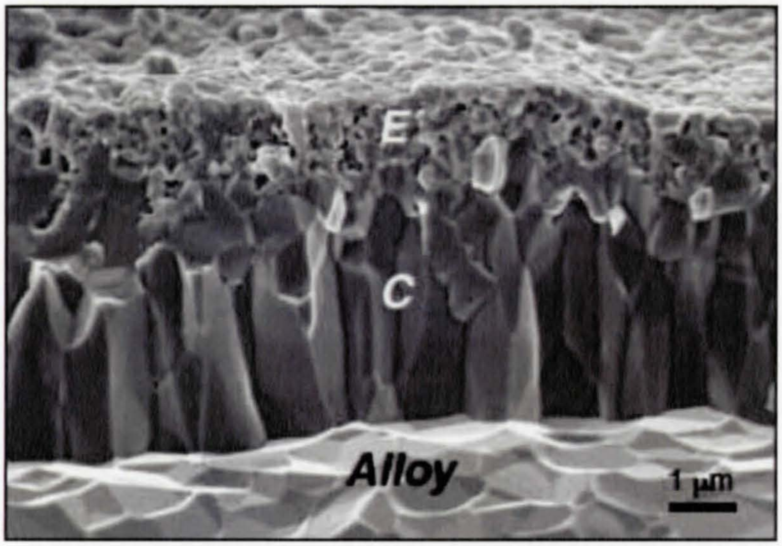

Figure 2.6: Fractured cross-section of Al_2O_3 scales after re-oxidation (Clarke, 2003)

Following the above mentioned work was Limarga et. al. (2004) Using the same principles set out by Rhines and Wolf (1970), Tolpygo and Clarke (2002), Nychka and Clarke (2005), and other notable researchers in this filed, they developed a one dimensional model based on the local diffusional fluxes of metal and oxygen ions that realistically and sufficiently estimates the magnitude of stresses induced during oxidation.

Construction involved analysis of stresses at both the grain boundaries of the scale and metal/oxide interface. This insured that the model kept with both the hypothesis defined by Rhines and Wolf (1970), and the experimental findings by Tolpygo and Clarke (2002) The geometry of the analyzed metal/oxide system is shown in Figure 2.7

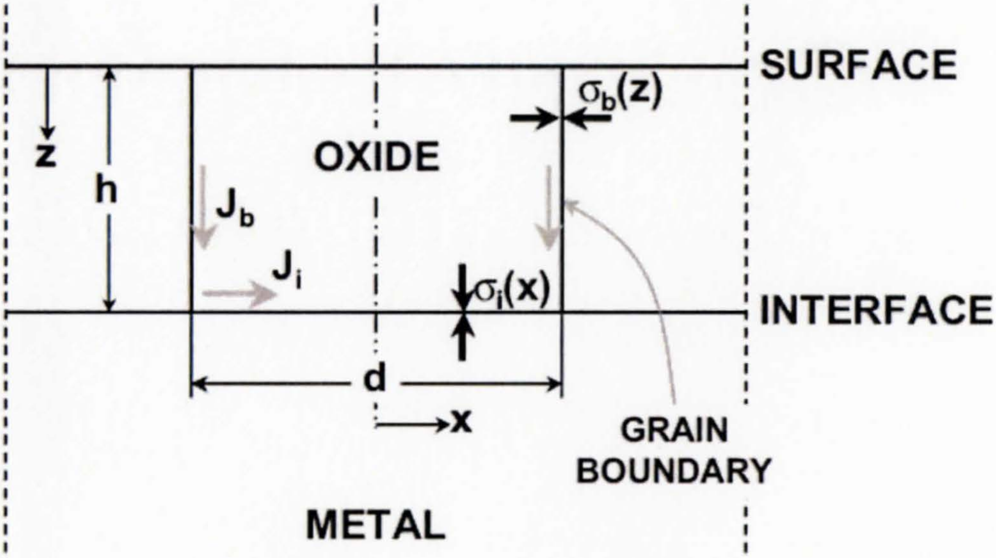

Figure 2.7· Geometry of the oxide/metal system analyzed (Limarga et al., 2004)

In this figure J is the diffusional flux, σ the stress induced during oxidation, d width of one oxide grain, and h height of the oxide grain from oxide/gas interface to metal/oxide interface. Subscripts b and i represent the grain boundary, and metal/oxide interface, respectively.

When considering the stress distribution at the metal/oxide interface, $\sigma_i(x)$, the profile was assumed to have a parabolic form with a common stress, σ_o, at $(d/2, h)$. This ensured that the deposition of new oxides was uniform along the interface. As such, the normal stress distribution acting on the metal/oxide interface is,

$$\sigma_i(x) = -\frac{6\sigma_o}{d^2}\left(\frac{d^2}{4} - x^2\right) + \sigma_o \tag{2.4}$$

Stress along the grain boundaries was determined using two distribution profiles, linear and constant (Evans et al., 1978), shown in Figure 2.8.

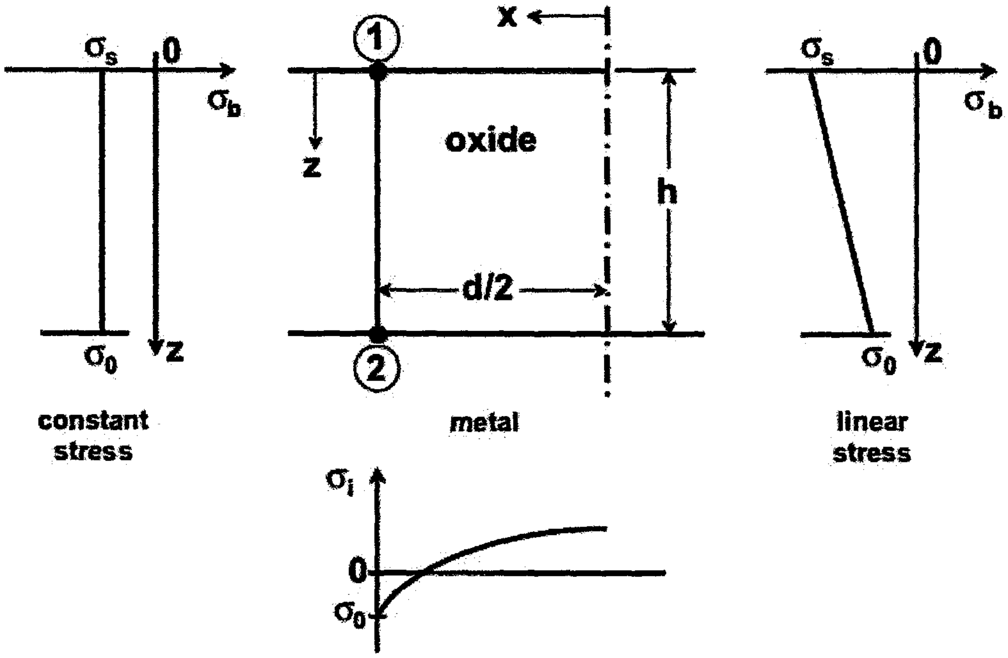

Figure 2.8: Stress distribution profiles along the grain boundaries (Limarga et al., 2004).

The stress profile for the case of linear stress distribution is expressed by,

$$\sigma_b(z) = (\sigma_o - \sigma_s)\frac{z}{h} + \sigma_s \tag{2.5}$$

where σ_s is the normal stress acting on the surface (position 1, $(d/2, 0)$, in Figure 2.8), and σ_o is the normal stress acting at the metal/oxide interface (position 2, $(d/2, h)$, in Figure 2.8). σ_s is represented by,

$$\sigma_s = -\frac{kT}{n\Omega_{ox}} ln \left[\frac{p(O_2)^g}{p(O_2)^{eq}}\right] \tag{2.6}$$

where $p(O_2)^g$ and $p(O_2)^{eq}$ are the partial pressure of oxygen at the free surface, and metal/oxide interface, respectively. σ_o is,

$$\sigma = -\frac{\frac{D_b}{h}}{\frac{D_b}{h} + 12\frac{D_i}{d}} \left\{ \frac{kT}{n\Omega_{ox}} ln \left[\frac{p(O_2)^g}{p(O_2)^{eq}}\right] \right\} \tag{2.7}$$

as the relationship between grain boundary and interfacial fluxes are defined by,

$$J_b = -2J_i \tag{2.8}$$

D_b and D_i are the constants for diffusion along the grain boundary and the metal/oxide interface, respectively.

The average of σ_o and σ_s give the stress profile within the scale,

$$\bar{\sigma}_{ox} = -\frac{kT}{2n\Omega_{ox}} ln \left[\frac{p(O_2)^g}{p(O_2)^{eq}}\right] \left[1 + \frac{1}{1 + \frac{12h}{d}\frac{D_i}{D_b}} \right] \tag{2.9}$$

Similarly, the average stress in a scale for constant stress distribution is determined by taking the average of σ_s and σ_o . Since it is assumed that the stress is uniform along the oxide grain boundary, the average stress within the scale is simply σ_o,

$$\bar{\sigma}_{ox} = \sigma_o = -\frac{kT}{6\Omega_{ox}} ln \left\{ \left[\frac{p(O_2)^g}{p(O_2)^{eq}}\right]^{\frac{1}{n}} \times \frac{D_b}{D_i}\frac{d}{2h} \right\} \tag{2.10}$$

The calculated results of Equations 2.9, and 2.10 are graphically shown in Figure 2.9 for Al_2O_3 scales. The considerable difference between the values for linear and constant stress profiles was attributed to the assumptions used in order to obtain a closed form solution. The experimentally determined values for growth stress (Tolpygo and Clarke, 1998a) for the same scale are also displayed, Figure 2.10. Comparison of the two results, theoretically calculated (Figure 2.9) and experimentally determined (Figure 2.10) growth stresses, shows good agreement; there is a small decrease in growth stress with increasing oxidation temperature. Note, this agreement refers to a very short oxidation period prior to stress relaxation (highlighted in Figure 2.10), which the model does not account for.

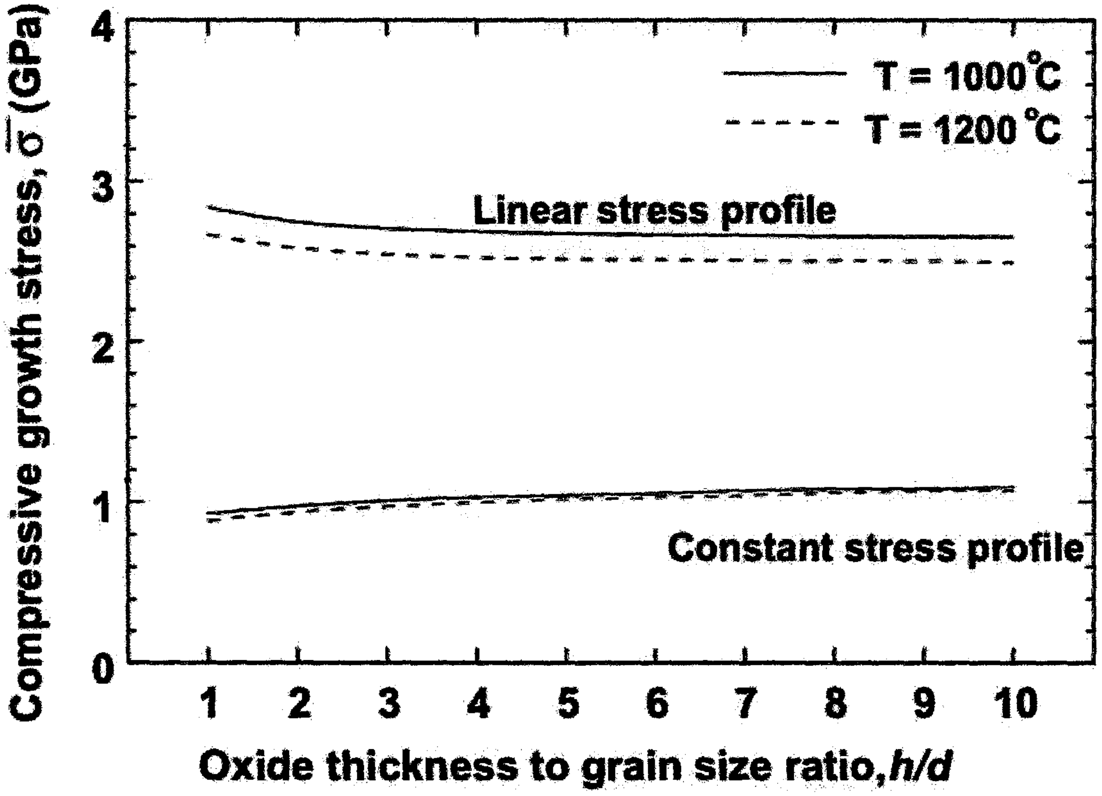

Figure 2.9: Calculated growth stress within Al_2O_3 scales, as a function of scale thickness to grain size ratio (h/d) (Limarga et al., 2004).

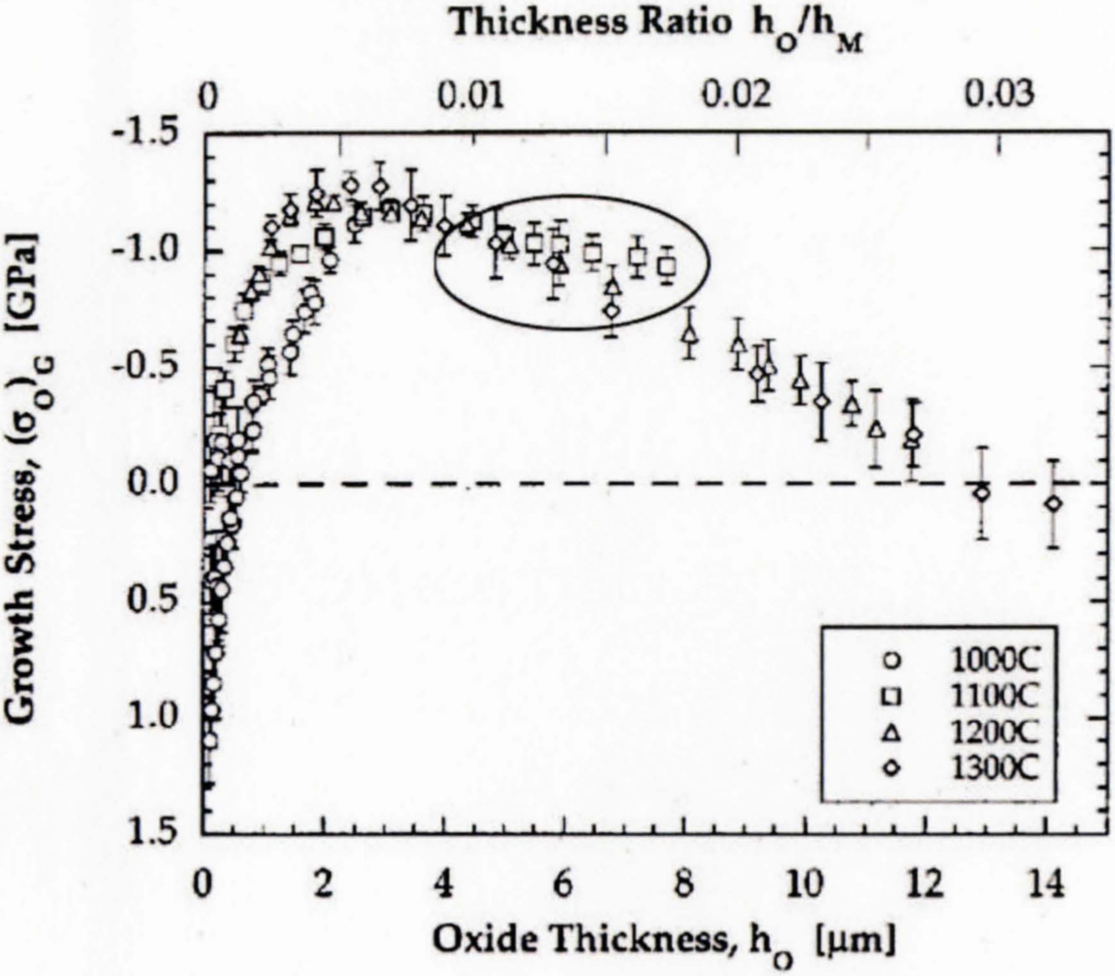

Figure 2.10: Experimentally determined growth stress as a function of oxide thickness, and ratio of oxide thickness to metal thickness for Al_2O_3 scales grown on FeCrAlY (Tolpygo and Clarke, 1998a).

It has been shown that although simple calculations can be performed to estimate thermally induced stresses, such calculations do not exist for oxidation growth stresses. Although, theoretical models (Limarga et al., 2004; Evans et al., 1978) have offered promise in providing closed form solutions for their calculation, there still exists a large uncertainty as to their validity. The reason is that the exact mechanism and defects responsible for oxidation-induced growth stress have not been conclusively determined. The difficulty lies mainly on the simultaneous and inseparable contributions of thermal and growth stress towards the measurement of residual stresses. Additional complications include concurrent stress relaxation that occurs during the oxide growth process, as discussed later.

Recent investigations have provided possible sources and concepts; most notably counter concurrent-diffusion of cations and anions through the grain boundaries of pre-existing scales. However, despites these advances, a tremendous amount of effort is still required until complete understanding of the intrinsic stress generation process is achieved.

Chapter 3

Relaxation of Compressive Stresses

Earlier studies showed several direct evidences of oxidation-induced stresses, namely the dimensional changes in thin metal sheets and cylinders, elongation of nickel rods, curling of a film when removed from it's metal substrate, bending of thin oxidized specimens, increase sheet area, etc. Additional evidence was the observation of increased spallation on the compressive side of a flexure sample, and wrinkling or convolution of alumina scales subjected to prolonged high temperature exposure (see Rhines and Wolf, 1970). The combination of these events with the known existence of compressive stresses in alumina scales, as reviewed in Chapter 2, leads to an argument that there is a competition between stress generation and stress relaxation during the scaling process. Since the most direct observations of stress generation have been dimensional changes in the metal substrate, it insinuates that an important relaxation mechanism is creep deformation (Evans, 1995).

This chapter is dedicated to reviewing how scale growth can lead to creep deformation of the metal/oxide systems. Initially, a general overview of creep deformation will be provided in order to allow for a better understanding of the chapter's core topic, oxidation induced creep deformation. Also, although the actual creep mechanisms responsible for deformation are yet to be determined, there have been findings that give significant insight towards its relationship to the oxidation process.

3.1 General Creep Behavior

Following the application of stress at an elevated temperature, materials will undergo time-dependent deformation defined as creep deformation. The extent of deformation during the course of creep is dependent on stress, temperature and the material. Although every material has its unique creep behavior, the comparison of each creep curve at a given constant load demonstrates certain features in common (Sully, 1949).

An ideal creep curve, as shown in Figure 3.1, commonly consists of four stages as follows:

1. **Instantaneous deformation**

   An initial elastic/plastic extension that appears upon application of the load.

2. **Primary Creep**

   Deceleration of creep rate due to structural alteration in the material acting to retard normal flow processes necessary for deformation.

3. **Secondary creep**

   A steady-state creep, whose strain rate is approximately constant, as highlighted in Figure 3.1.

4. **Tertiary creep**

   The final stage of creep. Development of defects internal/external leading to stress intensification and effectively accelerating the creep rate to rupture.

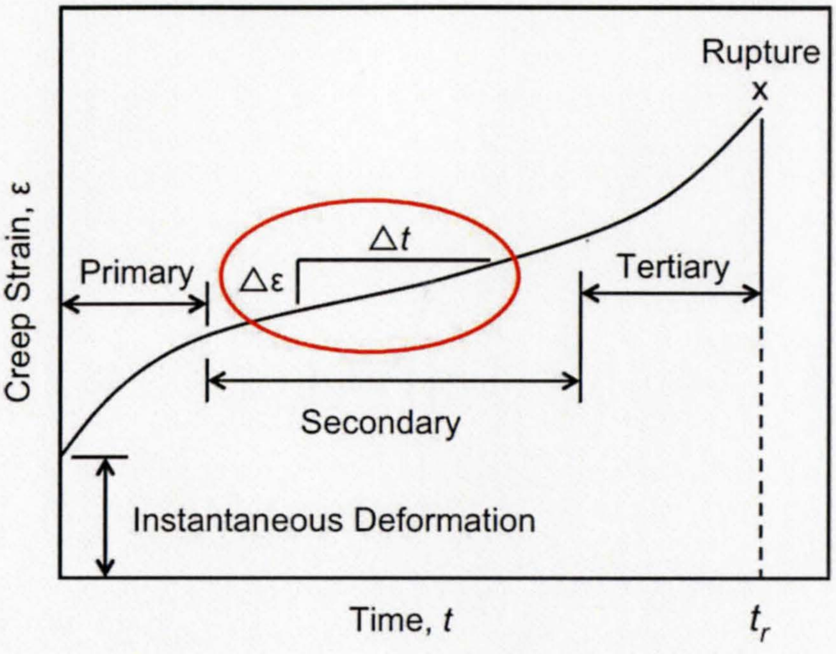

Figure 3.1. General creep curve at constant load.

Typically, for most materials in service, their constant load creep curve is distinguished by a prolonged stage of steady-state creep. In some instances, fracture, which is preceded by the tertiary stage, may not occur as the loads and given temperatures are too low to promote the onset of the third stage within the duration of the test. For the purposes of this work, applied loads, times and temperatures were selected to ensure that the specimen remained in the secondary creep stage and tertiary creep conditions were never met within the allotted time frame. As such only the secondary creep stage will be studied.

In brief, the relationship between stress and steady-state creep rate is expressed by the power law creep equation (Mennicke et al., 2001):

$$\dot{\varepsilon} \; = \; A\sigma^{n} exp\left(\frac{-Q}{RT}\right) \tag{3.1}$$

where $\dot{\varepsilon}$ is the steady–state strain rate, σ applied stress, A a constant that depends on microstructure, n stress exponent, Q activation energy for the process responsible for creep deformation, R universal gas constant and T absolute temperature. The slope of a double logarithmic plot of stress vs. strain rate gives the stress exponent. Additionally, the slope of a logarithmic plot of stress vs. inverse absolute temperature allows for the calculation of activation energy. It should be noted that by simply calculating the activation energy and stress exponent for a creep deformation curve, an accurate description of the creep mechanism involved cannot be sufficiently determined.

3.2 Oxidation-Induced Creep Deformation

Oxidation induced creep deformation can be explained by considering a metal substrate heated to high temperatures in oxidizing atmosphere as illustrated in Figure 3.2.

Initially, the metal will elongate inducing a lateral strain due to thermal expansion, $\alpha_m \Delta T$, where α_m is coefficient of thermal expansion for the metal and ΔT is the temperature difference from heating to cooling (Figure 3.2b). After a period, the substrate will form a thin oxide layer, which will grow and expand laterally by $\varepsilon_{ox}^{G}(t)$. Upon further oxidation lateral expansion of the oxide will be inhibited by the underlying substrate (Figure 3.2c). This constraint will create an in-plane biaxial compressive stress in the oxide layer, resulting in an elastic strain, ε_{ox}^{G}, where superscript G denotes oxide growth and subscript ox represents the oxide. Concurrently, the compressive stress will induce creep of the oxide, adding an additional strain, ε_{ox}^{Creep} (Tolpygo et al., 1998; Tolpygo and Clarke, 1998a, 1999).

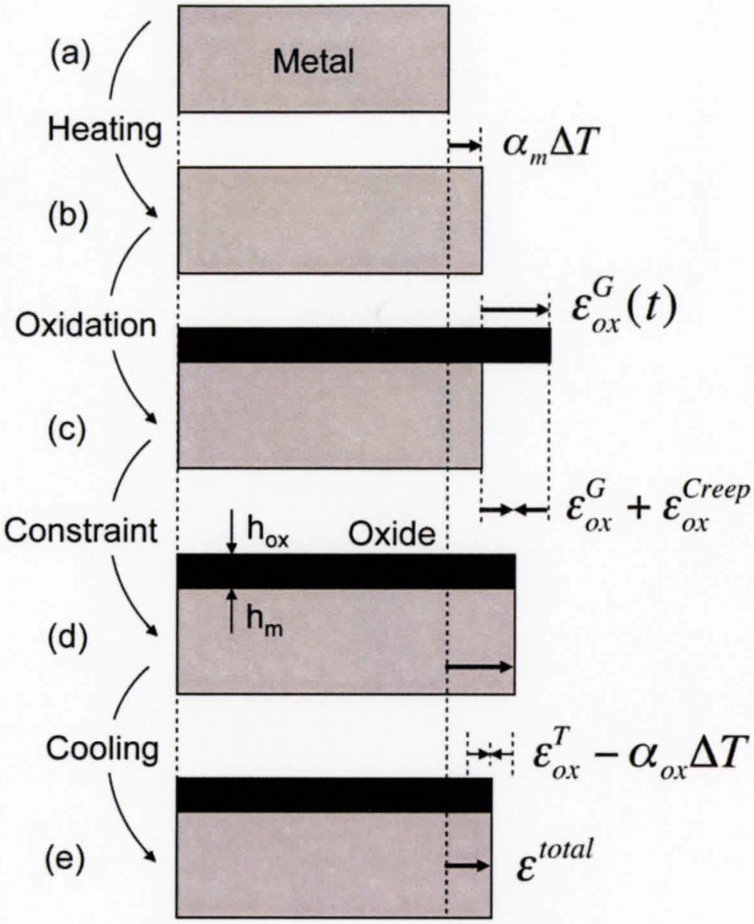

Figure 3.2: Schematic of deformation in a metal/scale system resulting from the scaling process (Tolpygo et al., 1998).

Once oxidation has stopped and the system has cooled to room temperature, assuming no plastic deformation has occurred during the cooling process, the scale will contract and therefore the compressive stress in the oxide scale is reduced by $\alpha_{ox}\Delta T$ Accompanying thermal contraction is thermoelastic strain in the oxide, ε_{ox}^{T}, brought on by the oxide and the metal being mutually constrained to one another Thus, the total strain in the oxide for an adherent metal/oxide system subjected to oxidation and cooling is as follows, ε_{ox}^{total}

$$\varepsilon_{ox}^{total}(t) = (\alpha_{ox} - \alpha_m)\Delta T + \varepsilon_{ox}^{G}(t) + \varepsilon_{ox}^{creep}(t) + \varepsilon_{ox}^{G} + \varepsilon_{ox}^{T} \tag{3.2}$$

In order to maintain mechanical equilibrium, which is the balance between compressive stress in the oxide and tensile stress in the metal, the total strain for the metal and oxide should be equal (Tolpygo et al., 1998).

In Equation 3.2, the last two terms represent the total oxide elastic strain at room temperature, described by the expression below:

$$\varepsilon_{ox}^{G} + \varepsilon_{ox}^{T} = \frac{\sigma_{ox}}{E_{ox}}(1 - \nu_{ox}) \tag{3.3}$$

where ε_{ox}^{G} is the elastic strain due to oxidation, ε_{ox}^{T} the elastic strain as a result of cooling, σ_{ox} the residual stress in the scale, determined experimentally, ν_{ox} the oxide's Poisson's ratio, and E_{ox} Young's modulus of the oxide (Tolpygo et al., 1998; Evans and Lobb, 1984). All the values of the aforementioned parameters are recorded at room temperature.

Assuming the oxide is very thin compared to the metal ($h_{ox}/h_m \rightarrow 0$), no relaxation occurs during cooling and the scale remains intact with the substrate, Hooke's law can be applied to Equation 3.3 giving an expression for calculating the intrinsic growth stress in an oxide scale at oxidation temperature,

$$\sigma_{ox} = \frac{E_{ox}}{E_{ox}^{T}}\sigma_{ox}^{G} + \sigma_{ox}^{T} \tag{3.4}$$

σ_{ox}^{G} is growth stress at oxidation temperature, σ_{ox}^{T} thermal mismatch stress in the oxide after cooling, σ_{ox} residual biaxial stress in the scale at room temperature, E_{ox} Young's modulus of the oxide at room temperature, and E_{ox}^{T}Young's modulus of the oxide at oxidation temperature (Tolpygo et al., 1998). Detailed derivation of the Equation 3.4 can be found in Appendix A.

Rearranging Equation 3.4 to obtain σ_{ox}^{G} and substituting into the force-balance argument, while maintaining the assumption that the h_{ox}/h_m approaches zero, tensile stress in the metal at oxidation temperature can be calculated (Equation 3.5).

$$\sigma_{ox}^{G} h_{ox} + \sigma_{m}^{G} h_{m} = 0 \tag{3.5}$$

If tensile stresses in the metal exceed the material's yield strength at oxidation temperature, the metal will ultimately extend and elongate to relax the tensile stresses, resulting in creep deformation. Such deformation in the metal was observed by Tolpygo and Clarke (1998) shown in Figures 3. 3ab.

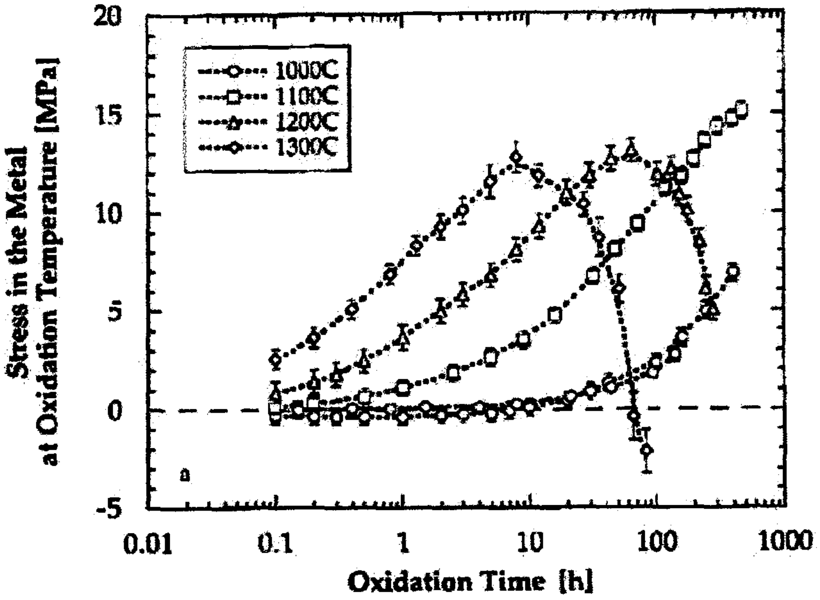

(a)

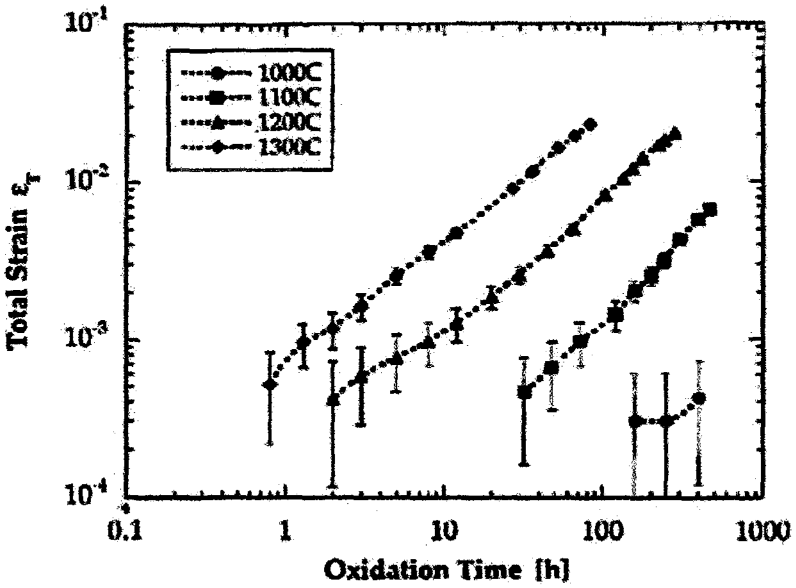

(b)

Figure 3.3: (a) Development of tensile stresses in the metal as a function of oxidation time, (b) total strain in the metal/oxide system as a function of time (Tolpygo et al., 1998).

Figure 3.3a depicts development of tensile stress in the metal as a function of oxidation time. The oxidation process occurs in a shorter time with increasing oxidation temperature. Moreover, yield strength of the metal at such high temperature decreases to about 1\5 of its maximum yield strength at room temperature, which allows for elongation at oxidation temperature, shown in Figure 3.3b. These evidences reaffirm the presences of stress relaxation in the oxide/metal system.

Another finding by Tolpygo et. al. (1998), shown in Figures 3.4ab, indicate that strain increases with increasing oxide thickness.

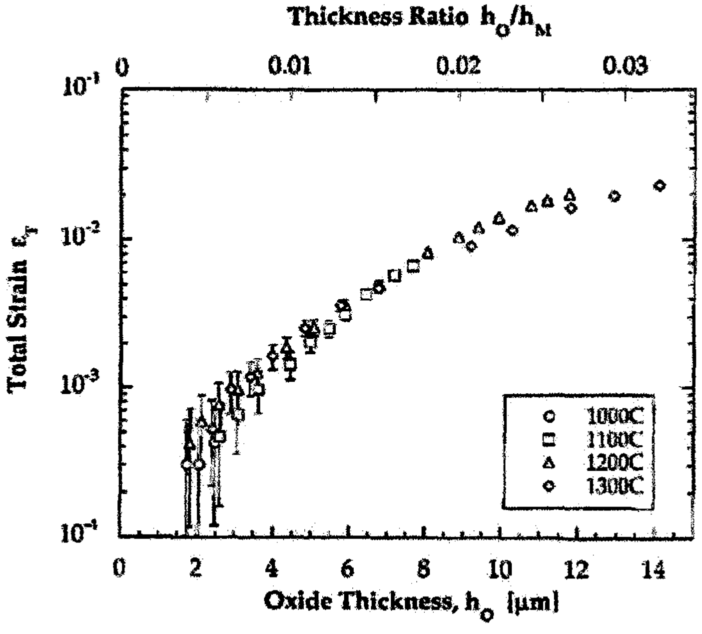

(a)

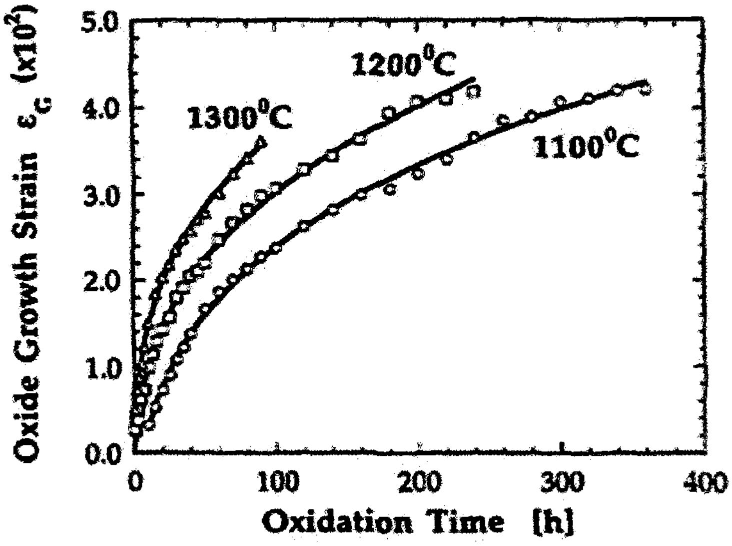

(b)

Figure 3.4: (a) Total strain in the metal/oxide system as a function of increasing oxide thickness (Tolpygo and Clarke, 1998a), (b) growth strain developed in the oxide scale as a function of increasing oxide thickness (Tolpygo et al., 1998).

In brief, oxide growth generates compressive stress in the scale, which eventually lead to tensile stresses in the metal inducing elongation of the metal substrate by creep deformation.

3.3 Stress-Induced Oxidation

Referring back to Figures 3.4ab, it is evident that increasing oxide thickness results in increasing strain in the metal/oxide system. Employing the reverse argument, it can be reasoned that oxide growth is influenced by strain, which is induced by stress relaxation at high temperature. Additionally, it can be inferred that since the development of tensile stresses in the metal due to the oxidation process is responsible for deformation, application of an external tensile stress would aid in oxide thickening, and a compressive stress will further hinder the process.

Exploring the above theory were Evans et al. (1978), where they proposed a model that examined the effects of stress on the oxidation kinetics in protective scales with respect to vacancy concentrations. They predicted that the oxidation controlling defects are in equilibrium at the oxide/metal and oxide/gas interface in the absence of stress. However, in the presence of stress the migration of defects responsible for oxidation may be influence and deferred from equilibrium.

Assuming that the flux of anion vacancies through the oxide is the rate limiting step for oxide growth, the chemical reactions in which vacancies are formed are then in equilibrium at both the metal/oxide and oxide/gas interface. During oxidation a solid volume change ($\Delta\Omega = \Omega_{ox} - \Omega_m$, transformation from a metal to oxide per ion) will occur, if this change is positive ($\Delta\Omega$ increases) a compressive stress (σ_{ox}) will be developed in the oxide. In order for oxidation to continue, work has to be done against this stress ($\sigma_{ox}\Delta\Omega$). This will displace the chemical reactions at the interfaces from equilibrium (Evans et al., 1978).

Since the diffusion rate of vacancies is determined by the their concentration, and since that concentration is stress driven, the diffusion rate of vacancies is also affected by stress. Therefore, the anion vacancy flux as influenced by stress is,

$$J_v \propto \frac{D_v}{h_{ox}} \left[C_{v,surface} - C_{v,interface} exp\left(\frac{\sigma_{ox} \Delta\Omega}{kT} \right) \right] \tag{3.6}$$

where D_v the vacancy diffusion constant, and $C_{v,surface}$ and $C_{v,interface}$ the vacancy concentration at the oxide/gas and metal/oxide interfaces, respectively. If the vacancy concentration at the metal/oxide interface is much greater than the concentration at the oxide/gas interface, then Equation 3.6 reduces to,

$$\frac{dh_{ox}}{dt} = \frac{D_{i,eff}}{h_{ox}} exp\left(\frac{\sigma_{ox} \Delta\Omega}{kT} \right) \tag{3.7}$$

where $D_{i,eff}$ is the effective diffusion coefficient for species i responsible for scale growth. In the absence of stress Equation 3.7 reduces to the classic parabolic law (Evans et al., 1978; Limarga and Wilkinson, 2006).

Further examination of Equation 3.7 suggests that in addition to growth stress, external compressive stresses would further influence the vacancy concentration, thus decreasing the oxide growth rate. It also implies that provided the accumulation of compressive stresses were sufficient, the oxidation growth rate could approach zero. On the contrary a tensile stress would create the reverse effect, increasing the oxide growth rate (Evans et al., 1978).

Support of the above mentioned observations and conclusions was provided in later years. Some mentionable investigations include:

- Rolls and Shahhosseini (1982) on Fe-Si alloys showed that the scale thickness of a stressed specimen doubled in comparison to an unstressed specimen. Their findings were attributed to the injection of vacancies into the substrate which reduced the concentration at the metal/oxide interface. This facilitated the climb process necessary for dislocation creep; thus, oxide growth stress was relieved, and oxidation growth rate was increased.

- Calvarin-Amiri et al. (2000, 2001) arrived at a similar conclusion to that of Rolls and Shahhosseini (1982), adding that the flux of vacancies into the substrate accommodated the volume increase required for continued oxidation.
- Toesca et al. (1981) on sulphidation of a FeCrAl alloy suggested that external tensile stresses caused an increase in through microcracks in scale. These microcracks exposed fresh metal to the harsh environment and allowed for further oxidation. Additionally, their observations showed that stress increased scale porosity, and small equiaxed grains. They proposed, later reaffirmed by Calvarin-Amiri et al. (2000, 2001), that porosity, boundaries of the equiaxed grains, and microcracks act as fast-diffusion paths for oxidation, all of which undoubtedly increases the oxidation rate.
- Limarga and Wilkinson (2006)on modeling the effects of bending and nitridation of $\gamma - TiAl$ showed that scale thickness increased on the tensile side, and decreased on the compressive side in comparison to unstressed specimens. Additionally, residual compressive stress in the scales was reduced on the tensile side of the specimen, and increased on the compressive side. Experimental work showed possible agreement.

In short, the aforementioned works and many others were in agreement with Evans et. al. (1978): the application of a mechanical load alters oxidation growth rates from its general parabolic trend to non-parabolic.

Chapter 4

Experimental Procedure

A previous study at McMaster University modeled the coupled effects of intrinsic growth stress and stress due to creep influences on scale growth rates in $\gamma - TiAl$. These works suggested that the application of tensile stress would increase the growth of a scale, while compressive stresses would reduce its growth rate. The experimental procedures and techniques outlined in this chapter have been designed and selected in order to better understand the relationship between scale growth rate, intrinsic growth stress and applied stress using the Fe-Cr-Al system.

4.1 Material Selection

The material selection was based on simple criteria: the material must form a simple uniform oxide, and counter diffusion of cations and anions must occur within the oxide layer promoting intrinsic growth stresses (see Section 2.2). Additionally, the material is to be doped with a reactive element in order to decrease oxide growth rate, increase scale adhesion and promote columnar structure, which is compact and protective (Stott, 1997; Jedlinski, 1997; Wilber et al., 2000).

In this study the chosen material was an iron-chromium-aluminum alloy, Kanthal Al, donated by National Electric Wire Company (New Jersey, USA). The composition of the alloy was given as 22 wt% chromium, 5.8 wt% aluminum with the balance being iron. Chemical analysis by glow discharge showed evidence of doping with zirconium, 0.1 wt%. X-ray diffraction pattern indicated that the material was single-phase and had a body centered cubic crystal structure, as shown in Figure 4.1. The material was supplied as an extruded 4' (1.22 m) rod approximately 0.560" (14.22 mm) in diameter. Due to the extrusion process the material's microstructure was highly deformed with large amounts of low angle grain boundaries, as shown in Figure 4.2.

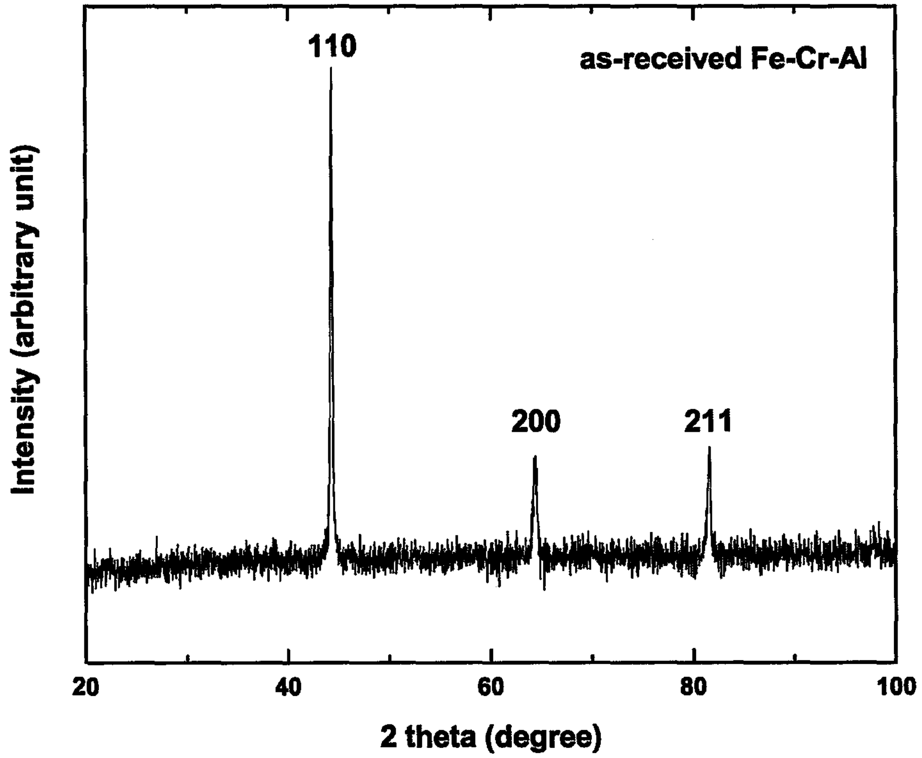

Figure 4.1: X-ray diffraction pattern of the as-received Fe-Cr-Al showing a single-phase body-centered cubic structure.

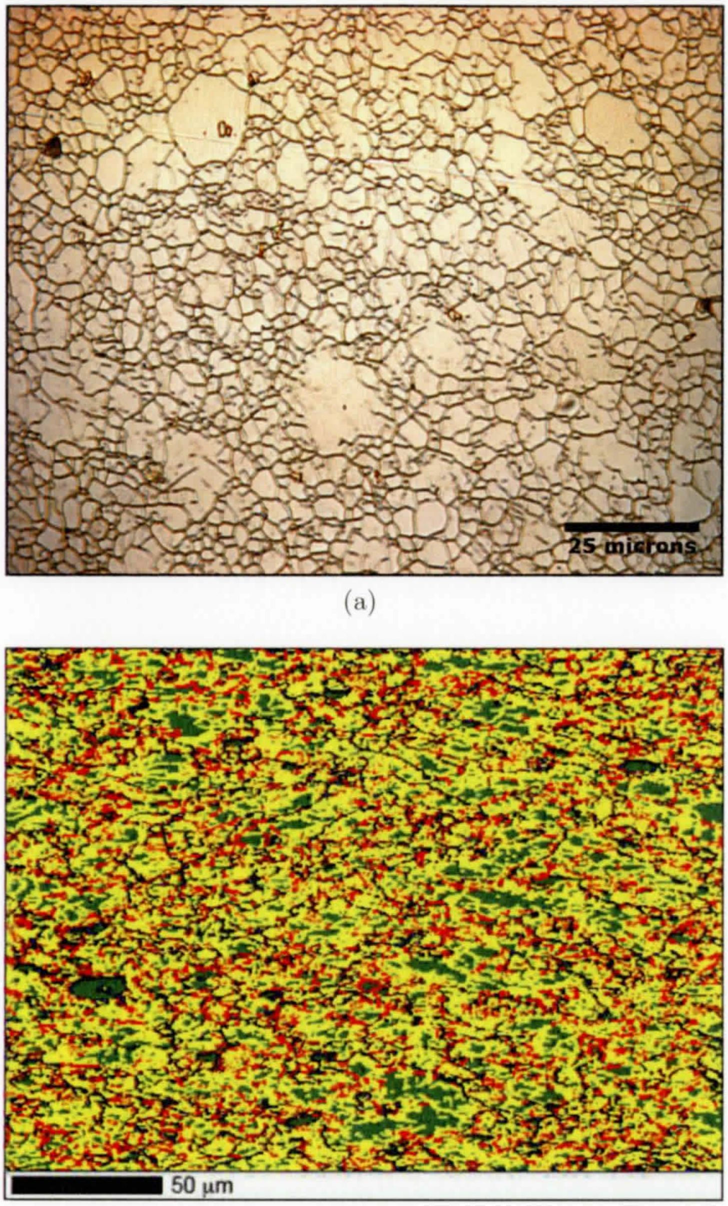

(a)

(b)

Figure 4.2: (a) Optical micrograph of as-received Fe-Cr-Al showing a highly deformed microstructure structure with non-uniform grains (b) Electron backscattered diffraction micrograph showing large amounts of low-angle grain boundaries as indicated by yellow area.

4.2 Sample Preparation

4.2.1 Creep and Oxidation

Two kinds of samples were machined: square samples (10 mm x 10 mm x 2 mm) for pure oxidation, and tensile samples for oxidation with applied stress. In order to achieve uniform oxidation and reduce contamination a hole was machined in the corner of the square sample so that it could be hung in the furnace with FeCrAl wire. A schematic of the square sample is shown in Figure 4.3a. The tensile sample was machined with a 19 mm radius at the gauge to ensure that elongation occurred at the center during creep testing. A schematic of the tensile sample is shown in Figure 4.3b (Carroll et al., 1989; Luecke et al., 1995).

A random grain structure was desired in order to eliminate the effects of substrate texture on scale morphology. To achieve this, both types of samples were annealed in argon gettered with zirconium for 24 hrs at 1200°C. Figure 4.4 shows an annealed square sample with random grain orientation. To obtain optimal residual stress measurements (among other measurements) and minimize surface roughness effects, the sample was further polished down to a 1 μm finish, ultrasonically cleaned in acetone, rinsed with ethanol, measured and weighed.

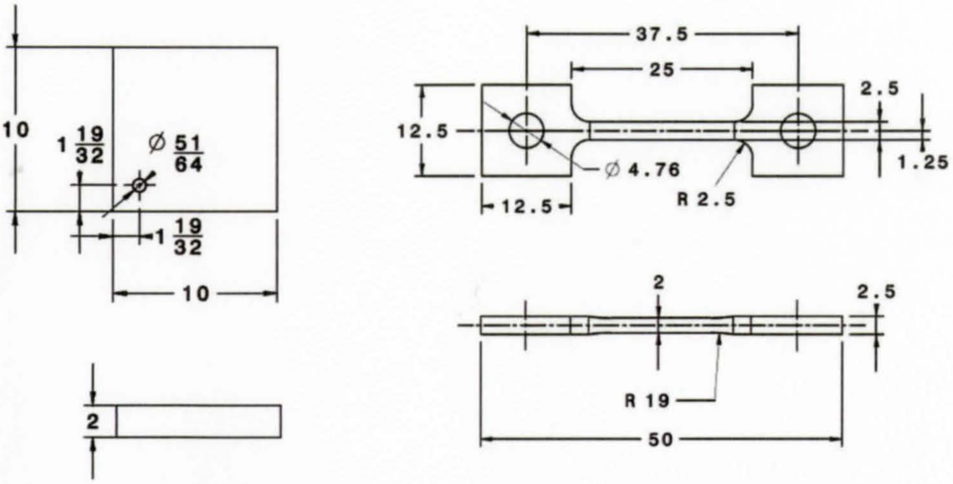

(a) Oxidation (b) Oxidation with applied load

Figure 4.3: Schematic diagrams of samples used for oxidation and creep test. All dimensions are in millimeters.

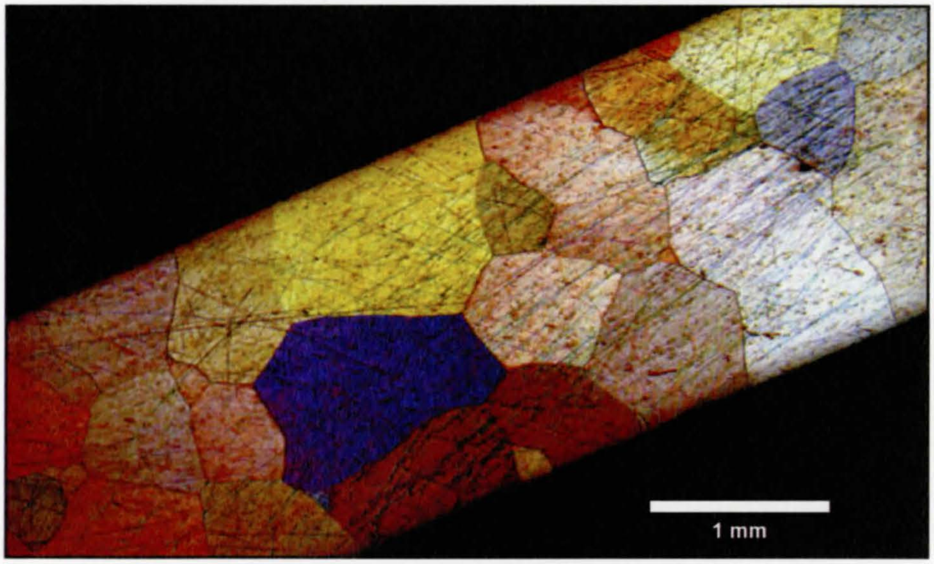

Figure 4.4: Optical micrograph of FeCrAl sample annealed in argon, gettered with zirconium for 24 hrs at 1200°C. Contrasting colors indicate random grain orientations. Image is obtained using cross-polarized light with Nomarski contrast.

4.2.2 Transmission Electron Microscope (TEM)

A TEM sample was prepared to determine the crystallographic phase of the thermally grown oxide (TGO). Typically x-ray diffraction (XRD) would be used for such characterization, however in this instance this technique could not offer conclusive evidence of the structure due to the TGO thickness being much smaller than the x-ray penetration depth. Therefore, a TEM specimen was prepared by carefully scraping the TGO from its substrate and crushing it into powder form. It was then diluted with ethanol into solution and sonicated. A drop of the solution was placed on a carbon TEM grid and left to dry.

4.3 Oxidation Experiment

A basic furnace equipped with two platinum thermocouples, furnace control and temperature overage, were used to oxidize the sample. A third thermocouple connected to a computer was placed near the sample to ensure that oxidizing temperature was within ±5°C. The sample was then dusted with air and hung in the furnace with FeCrAl wire. The furnace was insulated at the top and bottom with alumina wool in order to maintain a constant temperature. Oxidation was done at 1200, 1250, and 1300°C for 6, 12 and 24 hrs, with heating and cooling rates approximately 20°C/min and 7°C/min, respectively. Time started once the desired temperature was reached.

The chosen temperatures served two purposes. First, they maximized the compressive stress buildup in the scale within the time interval studied, which made for better residual stress comparison with the tensile samples. Temperatures below 1200°C were not suitable as maximum compressive stress could only be reached after 30 hrs or more of oxidation (Tolpygo et al., 1998; Tolpygo and Clarke, 1998a). Secondly, these temperatures ensured that only $\alpha - Al_2O_3$ scales were formed, simplifying required analysis of the scale (Stott, 1997).

4.4 High Temperature Tensile Creep Experiment

A direct load creep setup was used to perform the creep test in the same furnace setup as above (Section 4.3). Creep specimens were placed between two SiC pull rods. The bottom pull rod was connected to a weight pan where an additional load was placed, see Figure 4.6. The total weight acting on the sample included all parts connected below the sample.

A scanning laser extensometer (Beta LaserMike, Ohio, USA) connected to a computer terminal was used to monitor elongation of the gauge length marked by two SiC flags. The laser passed through a quartz window and the flags, forcing the beam to split into five segments as shown in Figure 4.5. Segment #2 and #4, seen in Figure 4.5, were formed as a result of the beam hitting the flags preventing light from reaching the detector. Elongation of the sample was measured by recording the increase in segment #3. Measurements were taken every 10 s and for every 0.001 mm increase in segment #3. Accuracy of each recording as reported by Beta LaserMike was ±2 μm. Creep testing was done at 1200 and 1250°C for 6, 12, and 24 hrs.

The experimental temperature 1300°C was excluded, as preliminary oxidation results showed that the formed scales were highly porous and non-uniform. An external stress would further increase porosity, and greatly affect residual stress measurements, i.e. findings would be meaningless (see Section 3.3, and Section 4.6).

The applied stress was 1.177 MPa (600 g) for 1200°C, and 0.785 MPa (400 g) for 1250°C. Due to the high oxidation temperatures, these were the maximum stresses that could be applied without causing fracture during testing or extensive strain that could lead to fracture during cooling. Fracture, by any means, would relieve the residual compressive stress in the scale, and lower the true calculated intrinsic growth stress. Any comparative findings (between pure oxidation and oxidation with creep) from the sample would cause uncertainty, particularly with regards to the effect of external stress on scale growth stress.

Tensile creep strain was calculated using an engineering strain expression:

$$\varepsilon(t) = \frac{l(t) - l_o}{l_o} \tag{4.1}$$

where $\varepsilon(t)$, $l(t)$ and l_o are the strain, gauge length and initial length, respectively.

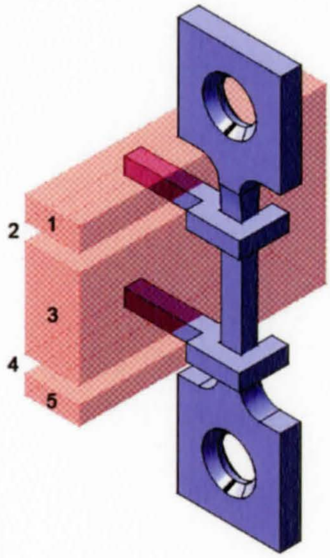

Figure 4.5: Schematic diagram showing the measurement of elongation by laser scanning extensometer

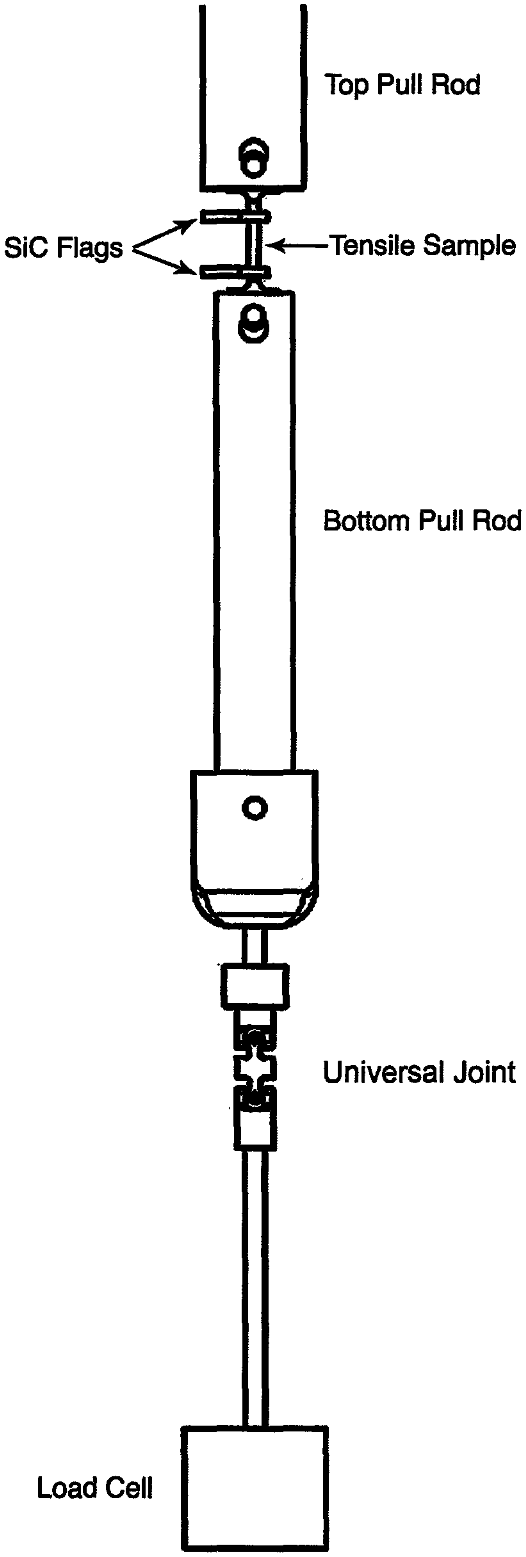

Figure 4.6: Schematic diagram of creep setup.

4.5 Electron Microscopy

4.5.1 Crystallographic Phase Analysis

Crystallographic phase of the oxide was characterized using selected area diffraction (SAD) on the TEM CM12 (Philips, Netherlands) at 120 keV acceleration voltage. The SAD pattern was indexed using JCPDS 81-1667 as a standard.

The *d*-spacing from the SAD patterns were calculated using:

$$R \cdot d = \lambda \cdot L \tag{4.2}$$

where L is camera length (530 mm), λ is the relativistic electron wavelength (0.00335 nm), and R is the radius of the ring pattern (mm). The experimental d was subjected to a correction factor of 0.954 which was acquired from calibrating an ideal single crystal.

4.5.2 Oxide Thickness Measurements

Focused ion beam NVision-40 Dual Beam console (Zeiss, Germany) was used to determine the thickness of the oxide layer. Sites were milled perpendicular to the sample surface revealing the cross-section of the oxide, the metallic substrate and the metal/oxide interface, see Figure 4.7. Prior to milling a platinum band was deposited at the milling site. This allowed for clear identification of the oxide's edge, and ensured that accuracy of thickness measurements would not be compromised by re-deposition from the milling process. The oxide layer was measured from the metal/oxide interface to the oxide's edge. The viewing angle was compensated with software correction. Using the systems resolution, accuracy was determined as ±100 nm. five sites were milled, with five measurements per site, giving a minimum of 25 measurements for each sample. The results were reported as mean values and standard deviations for the total of 25 measurements.

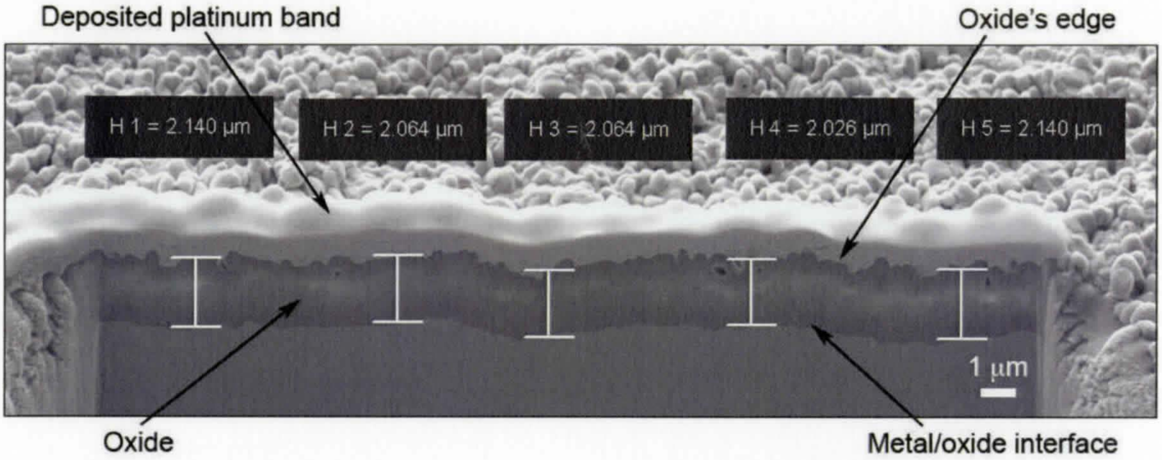

Figure 4.7: SEM micrograph showing FIB cross-section of $\alpha - Al_2O_3$ grown at 1200^oC for 6 hrs.

4.6 Residual Stress Measurement By Photo-Luminescence Piezo-Spectroscopy

Residual stress in the oxide was determined with photo-luminescence piezo-spectroscopy (PSLS) Andi Limarga, research associate in the Materials Department at the University of California, Santa Barbara, performed the measurements.

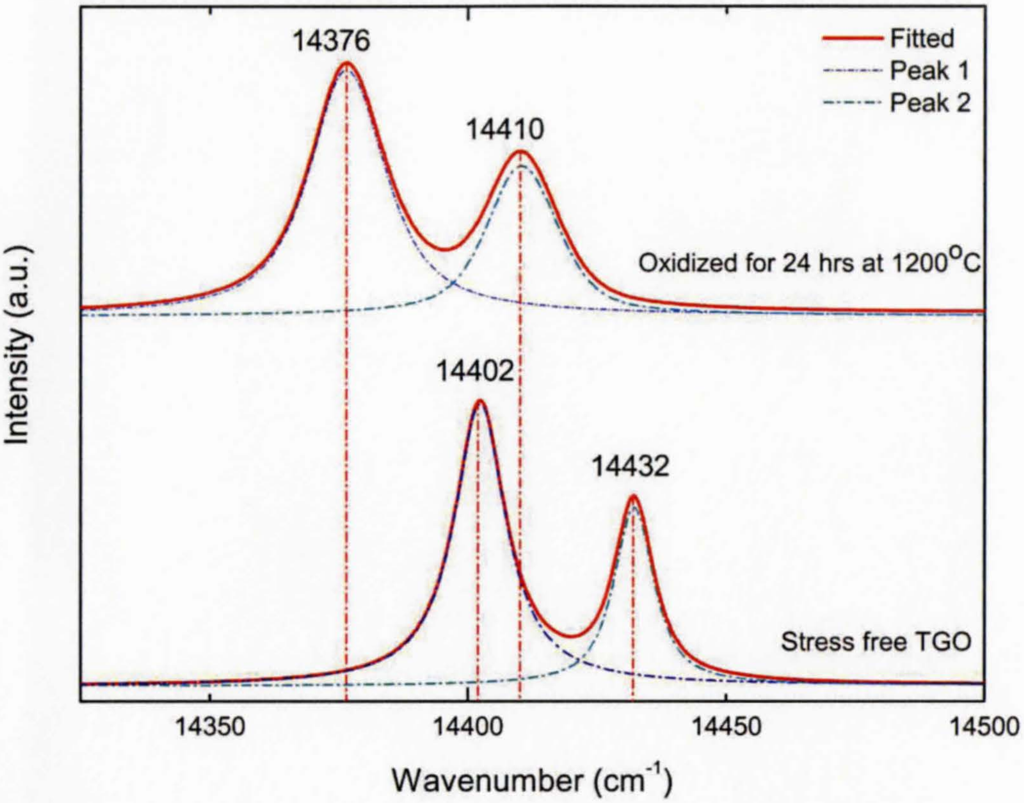

Figure 4.8: Fluorescence spectrum obtained from an Al_2O_3 scale on a FeCrAl sample oxidized for 24 hrs at 1200°C in air, and for a stress free Al_2O_3. The two lines and their respective frequencies are characteristic of the R-line fluorescence from Cr^{3+}-doped $\alpha - Al_2O_3$.

PSLS relies on the presence of chromium, Cr^{3+}, impurities in the α-alumina scale in order to produce the characteristic ruby-fluorescence R-line doublet. For a stress free α-alumina scale or sapphire crystal, the R1 and R2 occur at 14,402 cm^{-1} and 14,432 cm^{-1}, respectively. When Cr^{3+} in the oxide is stressed, the R-lines are systematically shifted, this is known as the piezo-spectroscopic effect (Lipkin and Clarke, 1996), shown in Figure 4.8. When this frequency shift, $\Delta\nu$, is relative to the characteristic R-lines in the stress-free alumina the local stress can be determined. The relationship between the frequency shift, $\Delta\nu$, and the local stress is expressed by,

$$\overline{\Delta\nu} = \frac{1}{3}\Pi_{ii}\sigma_{jj} \tag{4.3}$$

where Π_{ii} are the principal axis components of the piezospectroscopic tensor, Table 4.1, and σ_{jj} are the hydrostatic components of the applied stress tensor averaged over the probed volume (Lipkin and Clarke, 1996).

In Equation 4.3 only the principal axis values are required as the off-axis terms are comparatively negligibly small. Additionally, the above equation assumes that the material is polycrystalline and that the probe samples a sufficiently large ensemble of grains having random orientation (Lipkin and Clarke, 1996).

Table 4.1: Piezospectroscopic coefficients for Ruby (cm^{-1} /GPa) (Lipkin and Clarke, 1996)

Line	Π_{xx}	Π_{yy}	Π_{zz}	$\Pi_{xx} + \Pi_{yy} + \Pi_{zz}$
R1	2.56	3.50	1.53	7.51
R2	2.65	2.80	2.16	7.61

The piezospectroscopic tensor is a material-specific parameter. It reflects the point symmetry fluorescing ion in the host lattice.

For a flat scale, the stress is assumed to be biaxial, such that $\sigma_{xx} + \sigma_{yy} = \sigma$ and $\sigma_{zz} = 0$, where x and y are in-plane and z is normal to the surface, reducing Equation 4.3 to,

$$\Delta\nu = \frac{2}{3}\Pi_{ii}\sigma \tag{4.4}$$

and allowing for the frequency shift to be directly converted to a biaxial stress:

$$\sigma = \frac{3}{2}\frac{\Delta\nu}{(\Pi_{xx} + \Pi_{yy} + \Pi_{zz})} \tag{4.5}$$

where the term $(\Pi_{xx} + \Pi_{yy} + \Pi_{zz})$ is the trace of the piezospectroscopic tensor and has values of 7.59 cm^{-1} and 7.61 cm^{-1} for R1 and R2, respectively (Lipkin and Clarke, 1996).

For this study a He-Ne laser (633 nm) was used to excite the fluorescence. The spectrum was dispersed using a quad-grating spectrometer, LabRAM ARAMIS (Horiba Jobin Yvon, Edison, NJ) equipped with a CCD detector (Figure 4.9). A region of the scale was first selected using an optical microscope with a 50x objective. The laser beam was then focused through the objective lens on the selected feature giving a spot size of 10 μm. This spot size provided a better average of the stress due to the increase in probed volume, however spatial resolution was reduced. The excited fluorescence spectrum was analyzed with LabSpec (Horiba Jobin Yvon, Eddison, NJ) and GRAMS (Thermo Electron Corp., Philadelphia, PA). The fluorescence line positions and widths were obtained by fitting the spectra to a double-pseudo Voigtian functions, one for each of the R-lines.

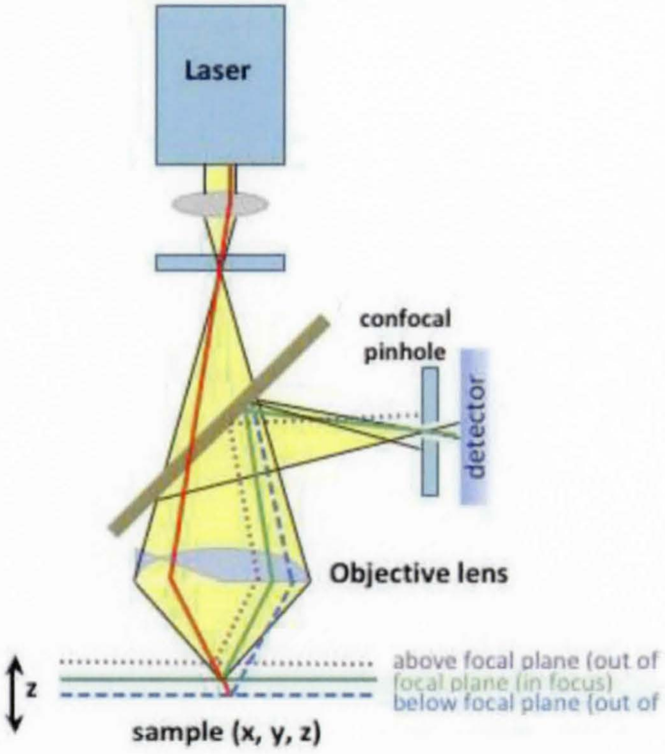

Figure 4.9: Schematic of Photo-Luminescence Piezo-Spectroscopy setup (Limarga, 2008)

Using Equation 4.5 the biaxial stress was calculated with Π-trace for R2. The R2-line is preferred for stress determination as the R1-line appears to show non-linearity in peak shift, especially for larger stress values (Limarga, 2008). The average values of the residual stress were determined from five individual measurements performed at different positions for each sample. Each measurement contained an inherent error 0.2 cm^{-1}, corresponding to about 40 MPa (Horiba Jobin Yvon, Eddison, NJ) Means and standard deviations were reported.

Chapter 5

Results and Discussion

This chapter will start with a general observation of the scales overall crystallographic nature, morphology and microstructure. Next, a detailed investigation and analysis on the scales thickness, measured residual stress, and calculated intrinsic growth stress as a function of time and temperature, with and without external stress will be reported.

5.1 Crystallographic Phase

In all oxidation experiments, with and without stress, $\alpha - Al_2O_3$ was formed on the metal substrate. The crystallographic phase of the oxide scale was conclusively determined by using selected area diffraction (SAD) technique in the transmission electron microscope. The corresponding SAD pattern shown in Figure 5.1 was used to measure the radius of ring patterns for calculating the *d*-spacing from Equation 4.2. Calculated and theoretical values for *d* are listed in Table 5.1. Experimental error percentage for *d* is less than 0.2% for each *d*-spacing, thus indicating good agreement with the theoretical *d*-spacing values for $\alpha - Al_2O_3$ in accordance with the standard JCPDS 18-1667.

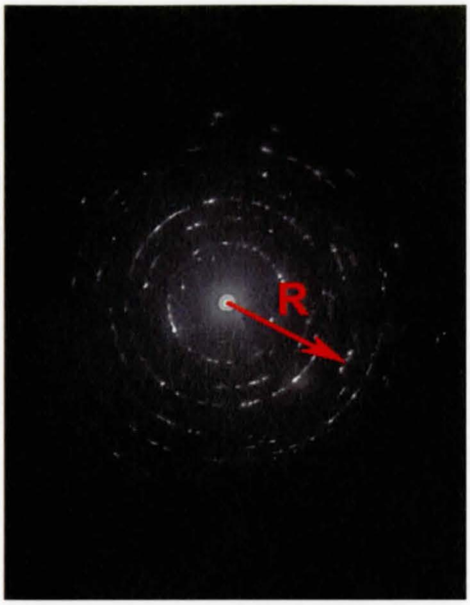

Figure 5.1. Selected area diffraction pattern for $\alpha - Al_2O_3$ scale oxidized for 6 hrs at 1200^{o}C.

Table 5.1. Calculated and theoretical d-spacings for the corresponding SAD pattern shown in Figure 5.1

(hkl)	$2R$ (mm)	d_{exp} (nm)	d_{theo} (nm)	$\Delta d/d_{theo}$ (%)
(0, 1, -4)	13.3	0.2547	0.2553	-0.2386
(0, 2, -1), (0, -2, -1)	16.6	0.2040	0.2037	0.1844
[0, 0, 9]	23.5	0.1442	0.1448	-0.2246
[0, 3, 6]	28.8	0.1176	0.1161	1.3151
(0, -4, 1), (0, 4, -1)	33	0.1027	0.1028	-0.1399
[0, 3, 9]	37.4	0.0906	0.0906	-0.0342

5.2 Microstructure

The microstructure of the scales cross-section was observed using a scanning electron microscope. The scales consistently exhibited a two-zone structure for all oxidation times and temperatures including samples oxidized with applied stress. The top layer was extremely porous with equiaxed grains, while the bottom layer was composed of compact elongated or columnar grains that extend from the metal/oxide interface, Figure 5.2.

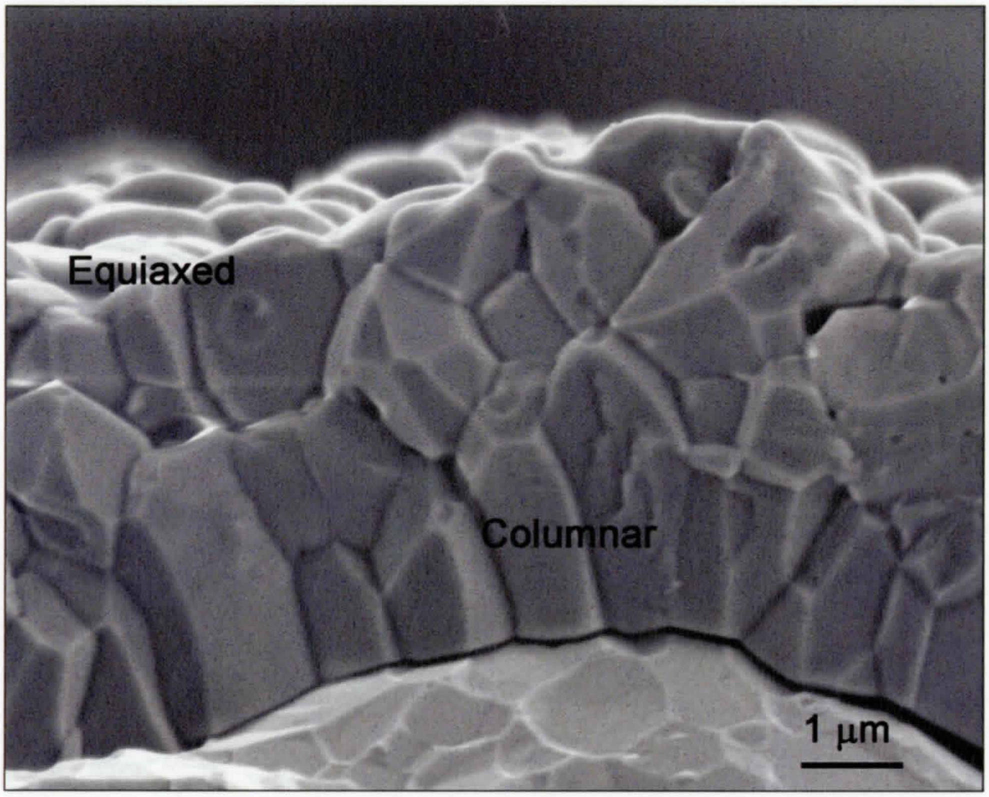

Figure 5.2: Freeze fractured cross-sectional SEM micrograph of $\alpha - Al_2O_3$ oxidized for 12 hrs at 1200°C.

As previously mentioned (see Section 2.2) the appearance of a two-zone oxide structure is an indication of concurrent counter diffusion of cations, Al^{3+}, and anions, O^{2-} Where Al^{3+} promotes outward scale growth distinguished by porous equiaxed grains, and O^{2-} contributes to the columnar zone, compact and fully dense. This counter diffusion of anions and cations is also responsible for the intrinsic growth stresses developed in the oxide. Since, such microstructure is present for all oxidation conditions, it is expected that the scales will have a considerable compressive growth stress (discussed in Section 5.5)

The evolution of microstructure development with respect to time and temperature without applied stress is displayed in Figure 5.3. The micrographs are arranged from left to right with increasing length of oxidation time (6, 12 and 24 hrs), and from top to bottom with increasing oxidation temperature (1200, 1250 and 1300^{o}C)

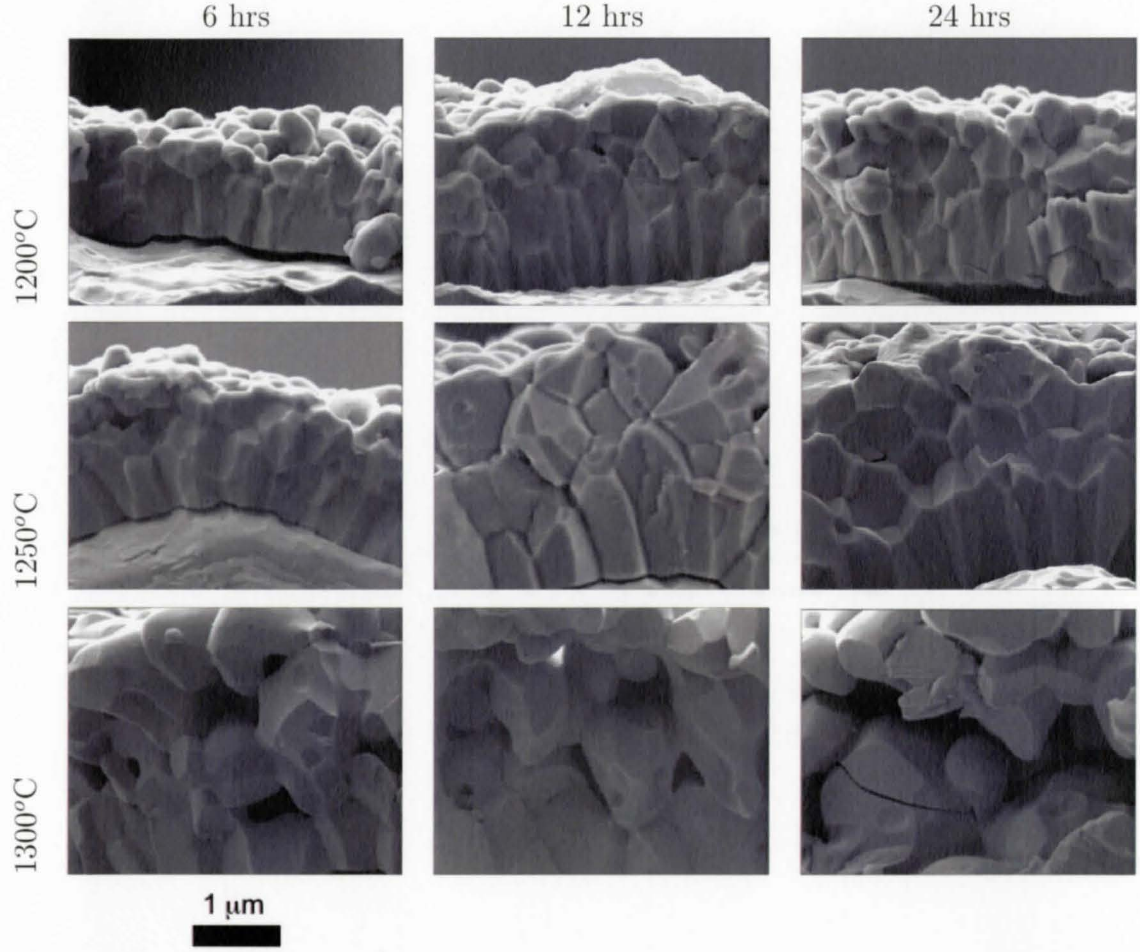

Figure 5.3: Freeze fractured cross-sectional SEM micrographs for samples oxidized without applied load. Images reveal the evolution of the scales with respect to time and temperature.

From these images it is obvious that scale thickens with both increasing time and temperature. Additionally, grain morphology, grain size and porosity of the scale also changes with oxidizing parameters. Most notably, the ratio of equiaxed to columnar grains is observed to be dependent on the temperature and length of oxidation.

At 1200°C for all times the microstructure of the oxide is flat and fully dense. Diffusion of anions, O^{2-}, appears to be dominant, as distinguished by mostly columnar grains with only a small top layer of equiaxed grains. Additionally, there appears to be no significant oxide thickness change with respect to increasing time, which indicates that oxide growth stress is relatively high and inhibiting further oxidation of the metal.

At 1250°C the microstructure is very similar to that at 1200°C. The scale is still dense, and relatively flat; however, there is a slight increase in porosity. This accounts for the change in ratio between the columnar to equiaxed zones, which is now about 1:1. Growth stress is expected to be smaller in comparison to samples oxidized at 1200°C.

At 1300°C the microstructure is significantly altered. The scales are almost mainly composed of highly porous equiaxed grains, and the scale surface exhibits a wrinkled structure. These features suggest that formation of the scales was mainly driven by diffusion of Al^{3+}. After 12 and 24 hrs intergranular cracks and partial decohesion from the substrate are present. Additionally, the 50°C increase in temperature showed a marked increase in scale thickness and grain size. This dramatic change is most likely attributed to the significant scale porosity, which reduces oxide growth stresses and accommodate continued scale growth.

A similar microstructural evolution of the scale is observed for conditions with applied stress (1.177 MPa for 1200°C and 0.785 MPa for 1250°C), as displayed in Figure 5.4. These micrographs are also are arranged in the same fashion to those above; from left to right with increasing length of oxidation time (6, 12 and 24 hours), and from top to bottom with increasing oxidation temperature (1200 and 1250^{o}C) All notable features were preserved under these conditions as compared to the above micrographs (Figure 5.3) at their respective times and temperatures.

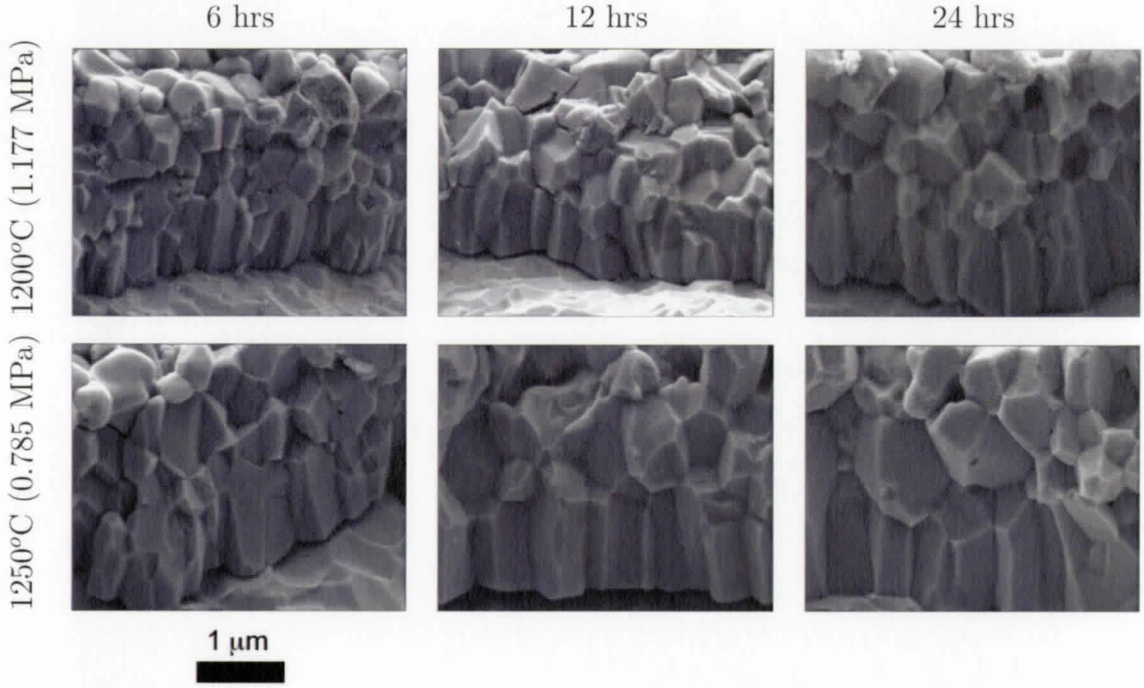

Figure 5.4: Freeze fractured cross-sectional SEM micrographs for samples oxidized with applied stress. Images reveal the evolution of the scales with respect to time and temperature.

For ease of comparison selected micrographs at 1250^{o}C without and with stress are displayed side by side in Figure 5.5 with increasing time from top to bottom (6, 12 and 24 hrs)

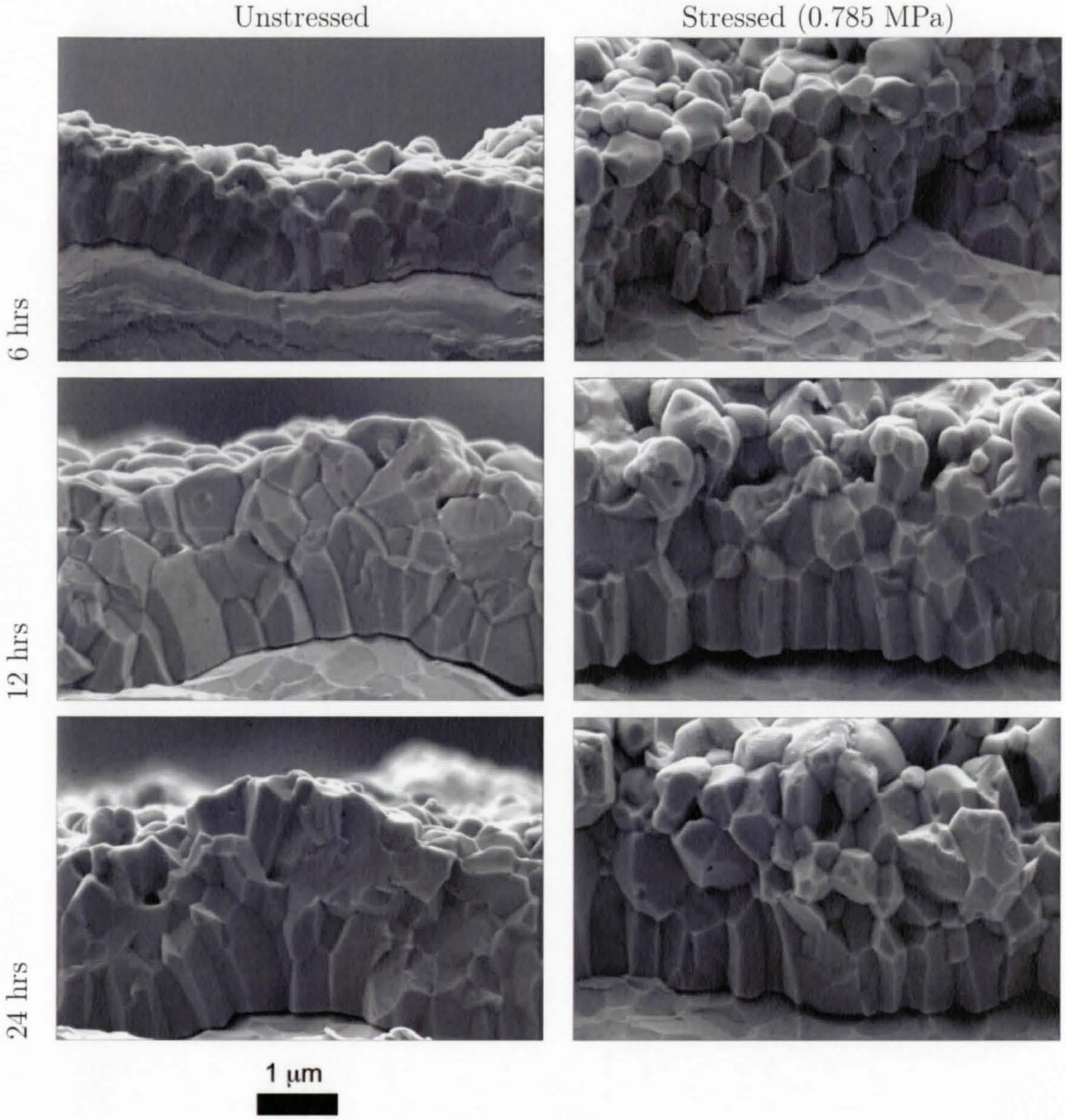

Figure 5.5: Comparison of scales microstructure between samples oxidized with and without stress at 1250°C for 6, 12 and 24 hrs. Applied stress was 0.785 MPa.

The most striking difference between each set of micrographs at the given temperature is the change in scale morphology and increase in porosity with increasing time. This suggests that the rate of scale growth of a specimen under tensile stress conditions is faster than that at rest. Furthermore, although not completely obvious, there is also a change in the ratio between columnar to equiaxed grains. Close examination of each micrograph for the stressed samples shows a larger equiaxed zone when compared to its unstressed counterpart. From this observation it can be assumed that tensile stress increased the diffusion of Al^{3+}. The implications of this observation is an expected decrease in growth stress.

5.3 Oxide Thickness

Compiled results of oxide thickness measurements for samples oxidized at 1200, 1250, and 1300°C for 6, 12 and 24 hrs are shown in Figure 5.6a. For comparison, thickness results for unstressed and stressed oxidation (1200°C with 1.177 MPa, and 1250°C with 0.785 MPa) are shown in Figure 5.6b.

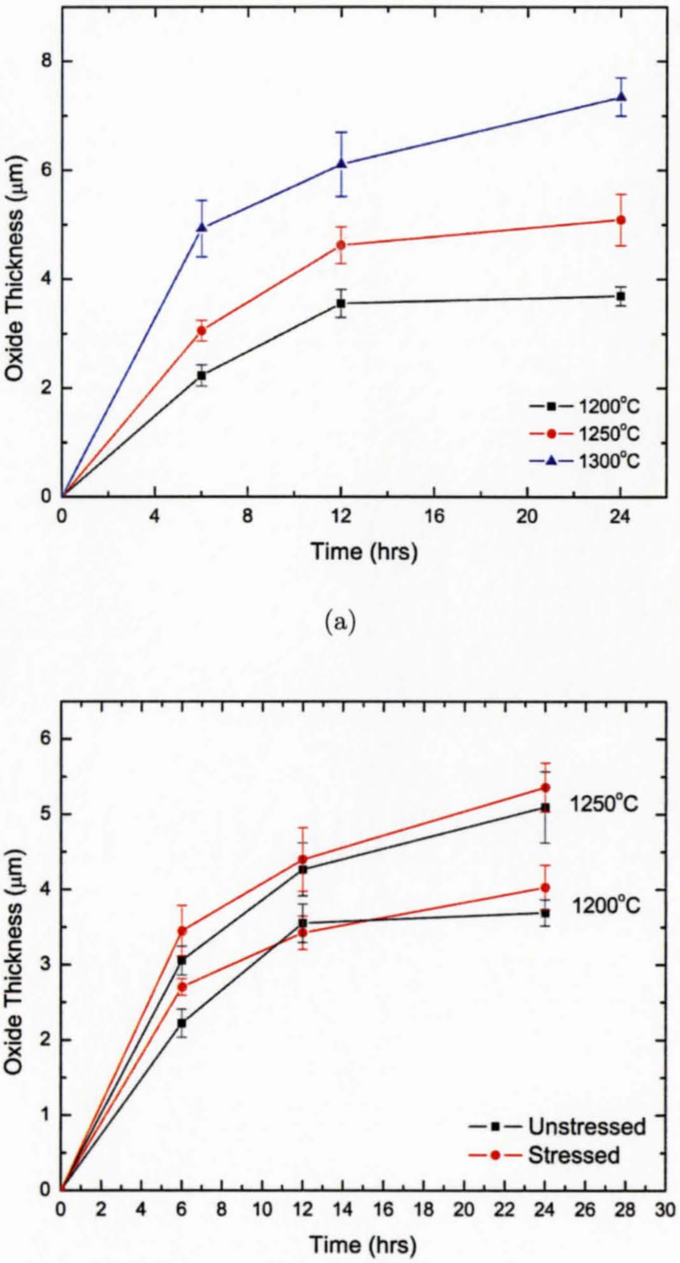

(a)

(b)

Figure 5.6: (a) Scale thickness as a function of time for samples oxidized at 1200, 1250 and 1300°C for 6, 12 and 24 hrs. (b) Comparison of scale thickness between samples oxidized with and without stress. At 1200°C applied stress 1.177 MPa and at 1250°C stress was 0.785 MPa.

The observed trend was as expected, increasing temperature and time lead to an increase in oxide thickness. However, the results for samples oxidized under stress were not according to expectations. It was anticipated that the application of a tensile stress would prevent the development of compressive stress that inhibited oxide growth, resulting in an increase in oxide thickness. Although, there appears to be a slight increase from 0 to 6 hrs, Figure 5.5b presents no significant change in oxide thickness thereafter. Despite microstructural evidence (Figure 5.5), conclusive statements with regards to a quantifiable effect that an external stress has on scale growth cannot be made, as values beyond 6 hrs fall very closely within experimental error. Possible explanations for this deviation from theory are discussed in Section 5.5.

5.4 Measured Residual Stress in $\alpha - Al_2O_3$ Scales

The measured residual stresses at room temperature for the oxides are shown in the Figures 5.7ab. Both figures reveal that residual stress is compressive and decreasing with increasing oxidizing times and temperatures. The range of measured compressive stresses lies between –5 GPa and –1.5 GPa. The highest stress value was observed at 1200°C after 6 hrs, and the lowest stress value at 1300°C after 12 hrs.

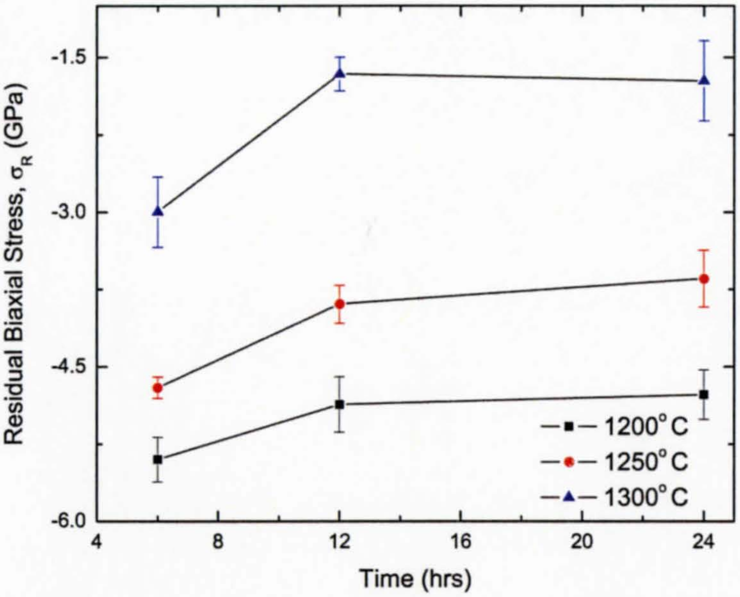

(a)

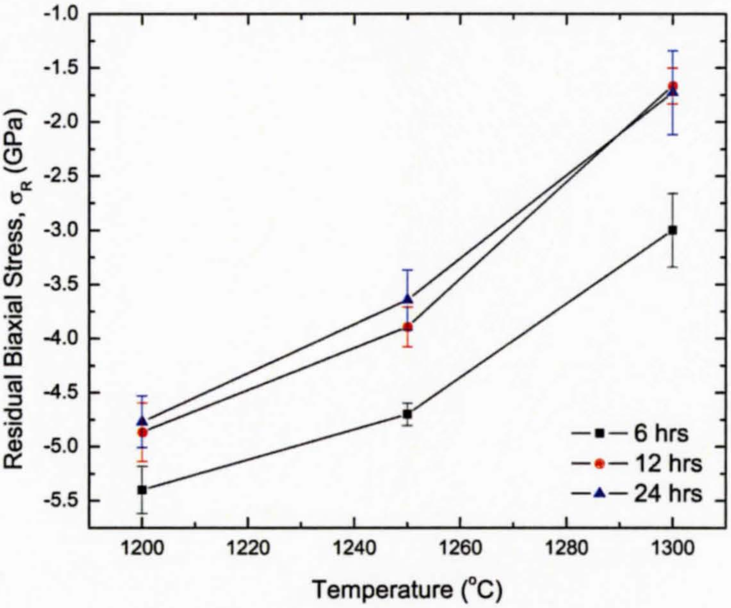

(b)

Figure 5.7· In-plane room temperature measured residual stress in $\alpha - Al_2O_3$ scales oxidized without applied load using PSLS. (a) Measured stress plotted as a function of time, (b) measured stress plotted as a function of temperature.

A comparison of the above results to samples subjected to an applied stress at 1200 and 1250°C are presented in Figures 5.8ab. For both oxidation temperatures, residual stress decreases with the application of a tensile stress. Based on these results, it is clear that an external tensile stress aids in the reduction of the compressive stresses in the scale by an order of 1 GPa.

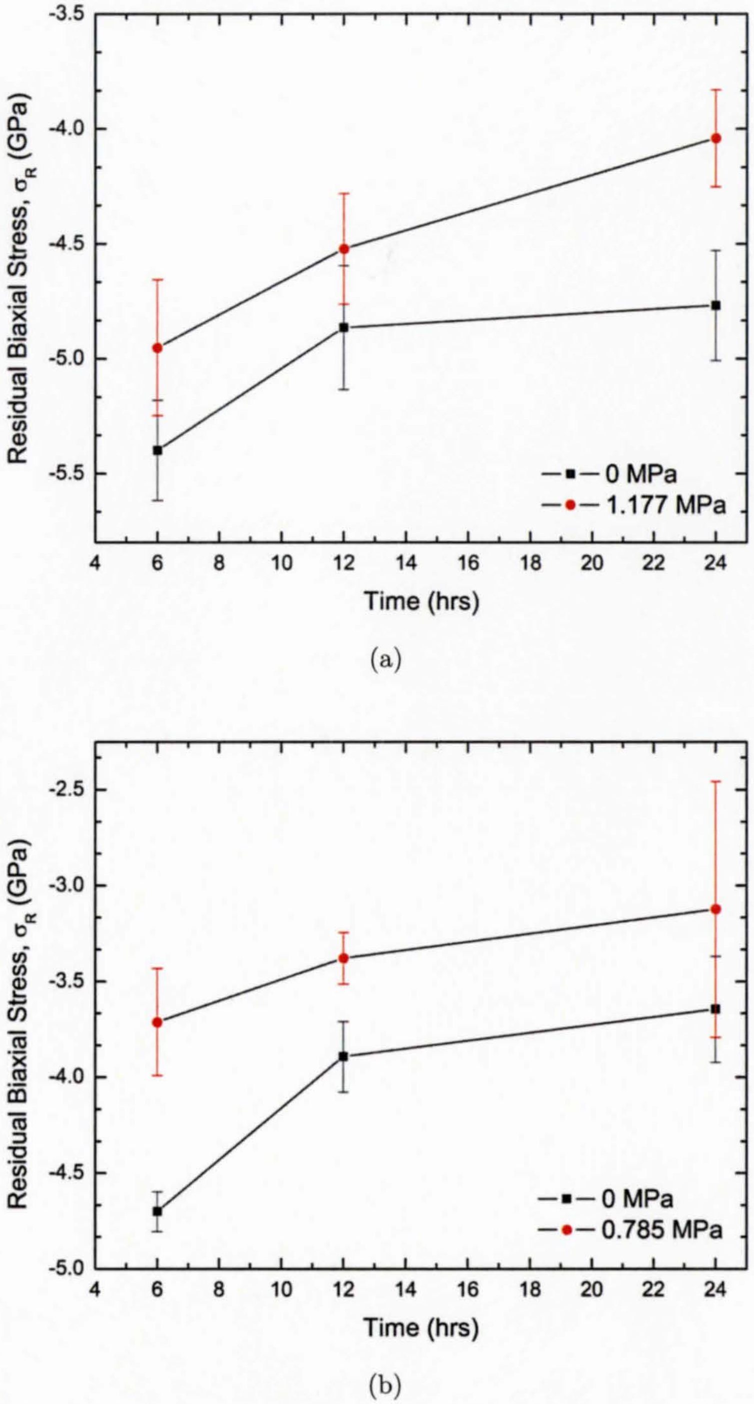

(a)

(b)

Figure 5.8: Comparison of residual stress between samples oxidized with and without applied load. (a) Samples oxidized at 1200°C with an applied stress of 1.177 MPa. (b) Samples oxidized at 1250°C with an applied stress 0.785 MPa.

The above results (Figures 5.7ab and 5.8ab) are consistent with those found in literature (Mennicke et al., 2001; Tolpygo et al., 1998). As the oxidation process proceeds, compressive growth stresses continue to buildup in the scale. This stress is balanced by a tensile stress in the substrate through the force balance argument (see Section 3.2). Upon cooling, an additional compressive stress is added to the scale, further increasing the tensile stress in the substrate. If the tensile stress exceeds the substrate's yield strength, the metal/oxide system will deform. Strain energy in the system will be released, and residual stresses relaxed.

Referring back to the micrographs in Section 5.2 for oxidation without stress (see Figure 5.3), a significant increase in porosity with increasing oxide thickness was observed. After 12 hrs at 1300°C partial scale decohesion and intergranular cracking was visible, Figure 5.9. These aforementioned features are means of strain energy relief, which causes the decrease in residual compressive stress with increasing scale growth.

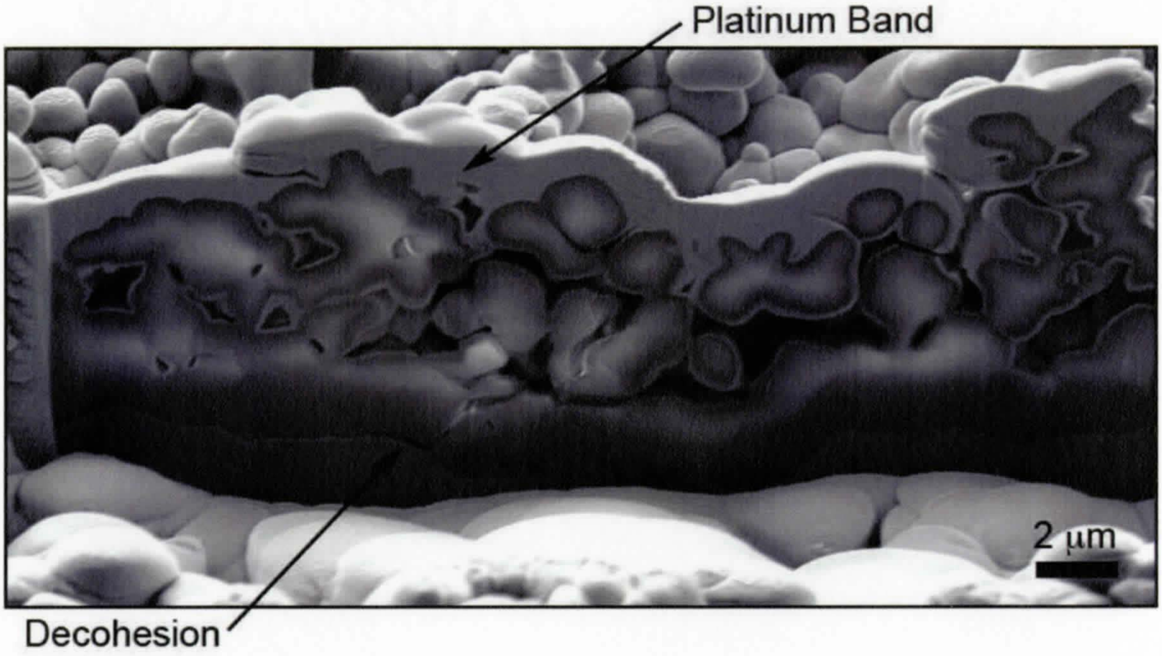

Figure 5.9: Cross-sectional FIB image of $\alpha - Al_2O_3$ scales oxidized at 1300°C for 12 hrs showing partial decohesion from the substrate.

For oxidation with stress, evidence of deformation is more apparent. Figures 5.10ab graphically demonstrates the decrease in residual stress with increasing deformation. For both temperatures, residual stress is lowest when strain is highest. This reiterates the notion that external tensile stress reduces residual compressive stresses in the scale.

A noteworthy mention is the similarity in trend between these observations to that of Tolpygo and Clarke (1998) The authors showed that residual stress decreased with increasing oxide thickness (see Figure 2.10) In this study residual stress decreased with increased deformation, applied stress (Figures 5.10ab) Thus, applied stress affects residual stress in scale in much the same way as scale thickening.

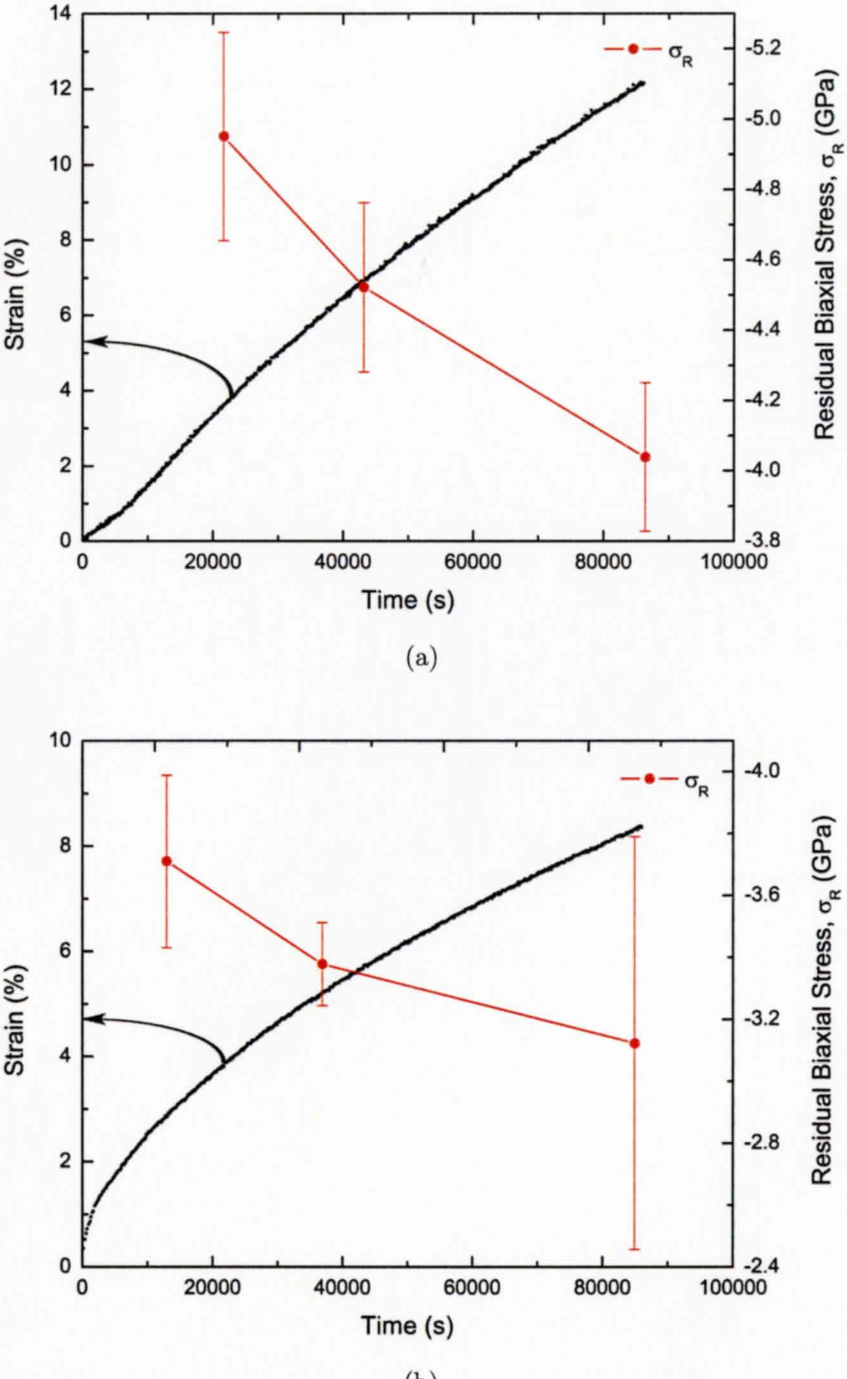

(a)

(b)

Figure 5.10: Illustration of effect of deformation of residual stress. (a) 1200°C with 1.177 MPa, (b) 1250°C with 0.785 MPa.

5.5 Calculated Intrinsic Growth Stress

The measured residual stress in the oxide scale is a combination of all possible stresses developed during the oxidation and cooling processes. It takes into account the stress due to thermal expansion mismatch between the growing oxide and metal, and growth stress due to oxidation.

Intrinsic growth stress at room temperature was calculated by manipulating Equation 3.4 in Section 3.2. Knowing the substrate and oxide's Young's modulus, measured residual stress values and the previously calculated thermal expansion mismatch stress listed in Table 2.1, the growth stress can be easily calculated. The results of calculated growth stress as a function of temperature and time are illustrated in Figures 5.11ab.

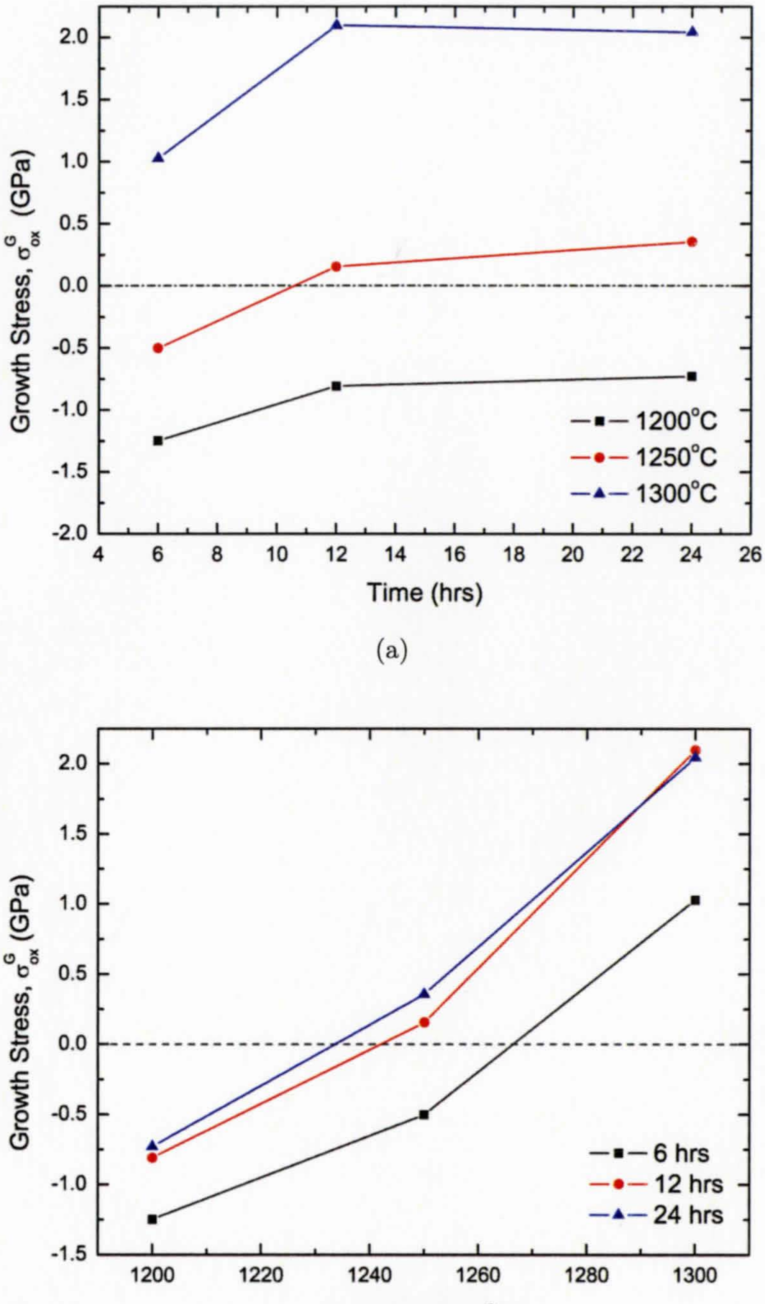

(a)

(b)

Figure 5.11. Calculated growth stress in $\alpha - Al_2O_3$ scales oxidized without applied load. (a) Calculated growth stress plotted as a function of time, (b) calculated growth stress plotted as a function of temperature.

The stress due to thermal expansion mismatch is evidently responsible for the accumulation of large residual stress in the scale (Figures 5.7ab). Since Equation 3.4 considers both growth and thermal expansion mismatch stress, removal of thermal stress significantly lowers the residual stress in the scale, and in some instances growth stress becomes tensile. Furthermore, evaluation of the two figures shows that intrinsic stress is more affected by temperature rather than time. With respect to temperature the calculated stress values differ by about 2.5 - 3 GPa, and with respect to time the stress values change only by about 0.5 GPa.

Comparison of growth stress without and with stress at 1200 and 1250°C are shown in Figures 5.12ab, respectively. The graphs clearly indicate that the application of a tensile stress during the oxidation process reduces the intrinsic growth stress of the scale. For experiments conducted at 1200°C growth stress is reduced by a maximum of 0.7 GPa, while at 1250°C maximum reduction reaches 1 GPa. Another important observation is that at 1250°C with applied stress, growth stresses are purely tensile.

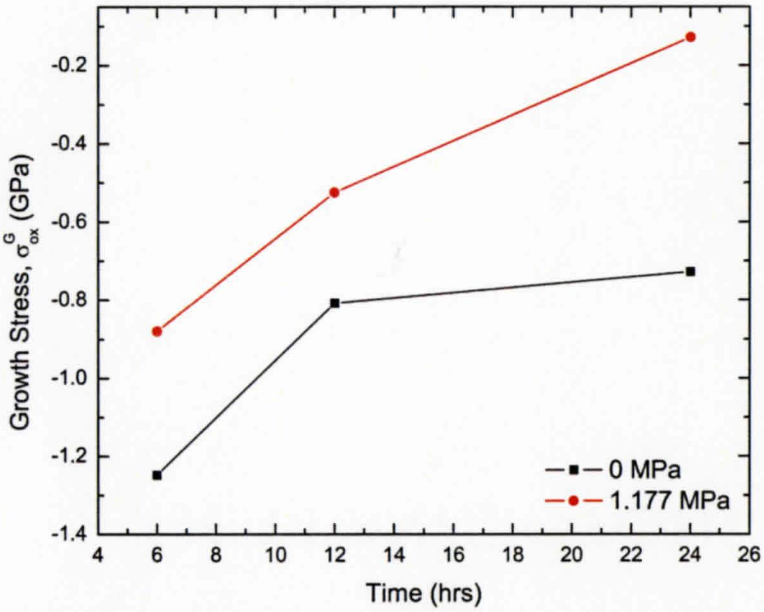

(a)

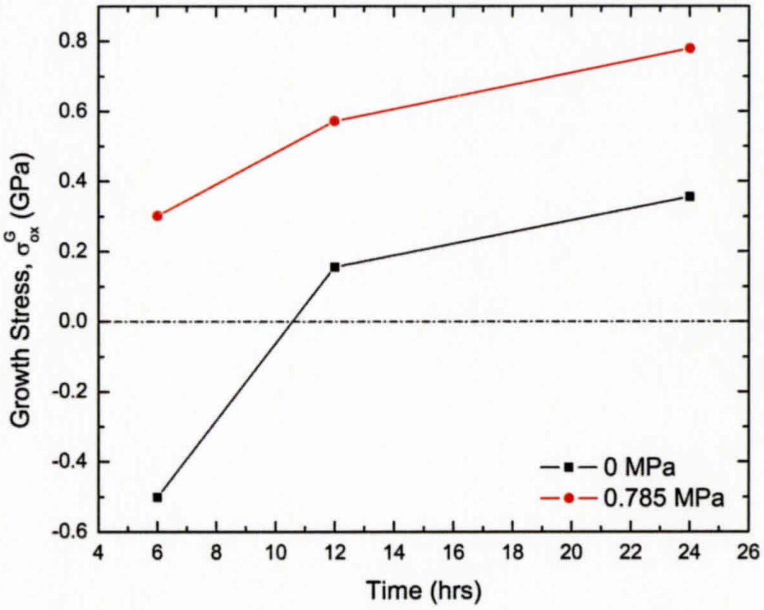

(b)

Figure 5.12: Comparison of calculated growth stress between samples oxidized with and without applied load. (a) Samples oxidized at 1200°C with 1.1772 MPa. (b) Samples oxidized at 1250°C with 0.785 MPa.

Theoretically speaking, such transition from compressive to tensile stress would give rise to a significant increase in scale growth rate with prolonged oxidation. Applying a tensile stress throughout oxidation would enable relaxation of growth stresses at a faster rate. With the increase in relaxation of growth stress, the scale can continue to grow and expand without being inhibited by adjacent grains (Section 3.2, and 3.3). However, such increase in scale growth rate was not convincingly evident in the experimental results described in Section 5.3 and Figure 5.6b. Based on current observations it is possible that the applied tensile stress was not sufficient to reduce intrinsic growth stress to magnitudes that would significantly increase the rate of scale growth, resulting in the negligible scale thickening.

Another plausible reason for the lack of scale thickening, is increased spallation. As previously stated, the microstructure of scales grown without stress showed a rise in porosity with both increasing time and temperature. Since tensile stress promotes outward scale growth, porous equiaxed grains, the already porous microstructure became more porous with applied stress. High porosity enables spallation. Spalling exposed the underlying metal to the oxidizing atmosphere allowing for further oxidation of the substrate. The new oxide grew and concealed all spalled sites. The process of oxide growth and spallation continue for the duration of the experiment. Consequently, additional increase in oxide thickness that might have been, was lost, resulting in unexpectedly low thickness measurements. This explanation, is also a viable cause for the almost steady scale growth rate observed for all temperatures above 12 hrs.

Chapter 6

Summary

The relationship between stress generation, stress relaxation, and external stress has been studied experimentally using an FeCrAl based alloy, Kanthal Al.

The formed scale under all oxidation conditions was confirmed to be a homogeneous alpha-alumina scale, with two distinct morphologies, the top layer was equiaxed and the bottom layer, adjacent to the metal substrate, was columnar. Such a dual phase structure indicates the existence of competing diffusing species across the scale. Initially, O^{2-} is the dominating diffusing species giving rise to more pronounced columnar grains that are adherent and flat. As the oxidation process continues the rate of diffusion between cations and anions becomes equal, indicated by the 1:1 ratio of equiaxed to columnar grains. At later stage of oxidation Al^{3+} is the more dominant species, which is represented by the increase in equiaxed grains that are porous and easily spalled.

Despite the reported service temperature for Kanthal Al of 1400°C, the experimental study indicated that the alloy was not suitable for oxidation above 1300°C in that it yielded a non-uniform porous and wrinkled scale. After 12 hrs the scale showed intergranular cracks and partial decohesion from the substrate, features that are detrimental to the alloys integrity.

Calculation of intrinsic growth stress in the oxide, from the measured residual stress values was easily carried out due to the simplicity of the single oxide system. The calculated intrinsic growth stress values showed a decreasing trend with increasing oxidation time and temperature. This trend was attributed to the increase in the scale porosity and wrinkling, which is a means of stress relaxation. Furthermore, the application of an external tensile load during oxidation decreased the intrinsic growth stress; however, it did not result in a meaningful increase in scale thickness as predicted. Possible rationale are insufficient tensile stress, and rapid spallation/re-healing during oxidation.

Based on the above mentioned summary there are a few suggestions pertaining to this study. As follows:

1. Differentiation of creep properties between the alloy and the formed scale is best done by performing separate experiments in vacuum and in an oxidizing environment.

2. Measurement of room temperature residual stress in the scale using PSLS is not advisable for oxidation experiments conducted at 1300°C or higher as the stress in the scale can no longer be considered in-plane biaxial.

3. Observation of the scale's grain morphology was best done by freeze fracturing the samples, as it revealed the ratio of columnar to equiaxed grains.

Appendix A

Calculation of Intrinsic Growth Stress

Compatibility of strains in the metal/oxide system at high temperatures is represented by Equation A.1.

$$\varepsilon_{ox}^{G}(t) + \varepsilon_{ox}^{Creep}(t) + \varepsilon_{ox}^{G} = \varepsilon_{m}^{Creep}(t) + \varepsilon_{m}^{G} \tag{A.1}$$

where ε_{ox}^{G} and ε_{m}^{G} are the elastic strains in the oxide and metal at high temperatures, $\varepsilon_{ox}^{G}(t)$ lateral growth strain in the oxide, ε_{ox}^{Creep} and ε_{m}^{Creep} are creep strains in the oxide and metal. Force balance at high temperature requires,

$$\frac{\varepsilon_{ox}^{G} E_{ox}^{T}}{(1-\nu_{ox}^{T})} h_{ox} = -\frac{\varepsilon_{m}^{G} E_{m}^{T}}{(1-\nu_{m}^{T})} h_{m} \tag{A.2}$$

$$\frac{E_{ox}^{T}(1-\nu_{m}^{T})}{E_{m}^{T}(1-\nu_{ox}^{T})}\frac{h_{ox}}{h_{m}} = R_1 \tag{A.3}$$

$$-\varepsilon_{ox}^{G} R_1 = \varepsilon_{m}^{G} \tag{A.4}$$

where E^{T} and ν^{T} are values at the oxidation temperature.

Substituting Equation A.4 into A.1 gives,

$$\varepsilon_{ox}^{G}(t) + \varepsilon_{ox}^{Creep}(t) + \varepsilon_{ox}^{G} = \varepsilon_{m}^{Creep}(t) - \varepsilon_{ox}^{G} R_1 \tag{A.5}$$

and rearranging gives,

$$\varepsilon_{ox}^{G}(t) + \varepsilon_{ox}^{Creep}(t) - \varepsilon_{m}^{Creep} = -\varepsilon_{ox}^{G}(1 + R_1). \tag{A.6}$$

The compatibility strains after cooling to room temperatures is as follows,

$$\varepsilon_{ox}^{G}(t) + \varepsilon_{ox}^{Creep}(t) + \varepsilon_{ox}^{G} + \varepsilon_{ox}^{T} + (\alpha_m - \alpha_{ox})\Delta T = \varepsilon_{m}^{Creep}(t) + \varepsilon_{m}^{G} + \varepsilon_{m}^{T} \tag{A.7}$$

where ε_{ox}^{T} and ε_{m}^{T} are the elastic strains for the oxide and metal due to cooling. Force balance at room temperature yields,

$$\frac{(\varepsilon_{ox}^{G} + \varepsilon_{ox}^{T})E_{ox}}{(1 - \nu_{ox})} h_{ox} = -\frac{(\varepsilon_{m}^{G} + \varepsilon_{m}^{T})E_{m}}{(1 - \nu_{m})} h_{m} \tag{A.8}$$

$$\frac{E_{ox}(1 - \nu_m)}{E_m(1 - \nu_{ox})} \frac{h_{ox}}{h_m} = R_2 \tag{A.9}$$

$$-(\varepsilon_{ox}^{G} + \varepsilon_{ox}^{T})R_2 = (\varepsilon_{m}^{G} + \varepsilon_{m}^{T}) \tag{A.10}$$

where E and ν are constants at room temperature.

Substituting Equation A.10 into A.7 gives,

$$\varepsilon_{ox}^{G}(t) + \varepsilon_{ox}^{Creep}(t) + \varepsilon_{ox}^{G} + \varepsilon_{ox}^{T} + (\alpha_m - \alpha_{ox})\Delta T = \varepsilon_{m}^{Creep}(t) - (\varepsilon_{ox}^{G} + \varepsilon_{ox}^{T})R_2 \tag{A.11}$$

and rearranging gives,

$$(\alpha_m - \alpha_{ox})\Delta T + \varepsilon_{ox}^{G}(t) + \varepsilon_{ox}^{Creep}(t) - \varepsilon_{m}^{Creep} = -(\varepsilon_{ox}^{G} + \varepsilon_{ox}^{T})(1 + R_2) \tag{A.12}$$

After applying Equation A.6, A.12 reduces to,

$$(\alpha_{ox} - \alpha_m)\Delta T = \varepsilon_{ox}^{G}(R_2 - R_1) - \varepsilon_{ox}^{T}(1 + R_2) \tag{A.13}$$

In order to determine the intrinsic growth stress in the oxide at high temperature, σ_{ox}^{G}, the expression for the total elastic strain at room temperature,

$$\varepsilon_{ox}^{G} + \varepsilon_{ox}^{T} = \frac{\sigma_{ox}}{E_{ox}}(1 - \nu_{ox}) \tag{A.14}$$

needs to be manipulated with Equation A.13 to give,

$$\varepsilon_{ox}^{G} = \frac{1}{(1 + R_1)}\left[\frac{\sigma_{ox}}{E_{ox}}(1 - \nu_{ox})(1 + R_2) - (\alpha_{ox} - \alpha_m)\Delta T\right] \tag{A.15}$$

which will then be simplified after Hooke's law has been applied giving the final expression,

$$\sigma_{ox}^{G} = \frac{E_{ox}^{T}}{(1 + R_1)(1 - \nu_{ox}^{T})}\left[\frac{\sigma_{ox}}{E_{ox}}(1 - \nu_{ox})(1 + R_2) - (\alpha_{ox} - \alpha_m)\Delta T\right] \tag{A.16}$$

Assuming that ν_{ox} is temperature independent, and h_{ox}/h_m approaches zero, Equation A.16 reduces to,

$$\sigma_{ox}^{G} = \frac{E_{ox}^{T}}{E_{ox}}\sigma_{ox} - \frac{E_{ox}^{T}(\alpha_{ox} - \alpha_m)\Delta T}{(1 - \nu_{ox})} \tag{A.17}$$

After simplifying and rearranging A.17 gives,

$$\sigma_{ox} = \frac{E_{ox}}{E_{ox}^{T}}\sigma_{ox}^{G} + \frac{E_{ox}(\alpha_{ox} - \alpha_{m})\Delta T}{(1 - \nu_{ox})} \tag{A.18}$$

where the second term on the right side the expression is the thermal mismatch stress in the oxide due to cooling, σ_{ox}^{T}. Thus Equation A.18 can be written as,

$$\sigma_{ox} = \frac{E_{ox}}{E_{ox}^{T}}\sigma_{ox}^{G} + \sigma_{ox}^{T} \tag{A.19}$$

(Tolpygo et al., 1998)

Appendix B

Mechanism of Deformation

Microstructural analysis of the surface of samples oxidized with applied load at 1200 and 1250°C for 6, 12, and 24 hours revealed the presence of cracks, and spallation particularly along the grain boundaries of the uplifted grains (Figure B.1). These features were not present in samples oxidized under the same conditions without applied stress. As oxidation time increased, the above features became more prominent (Figure B.2).

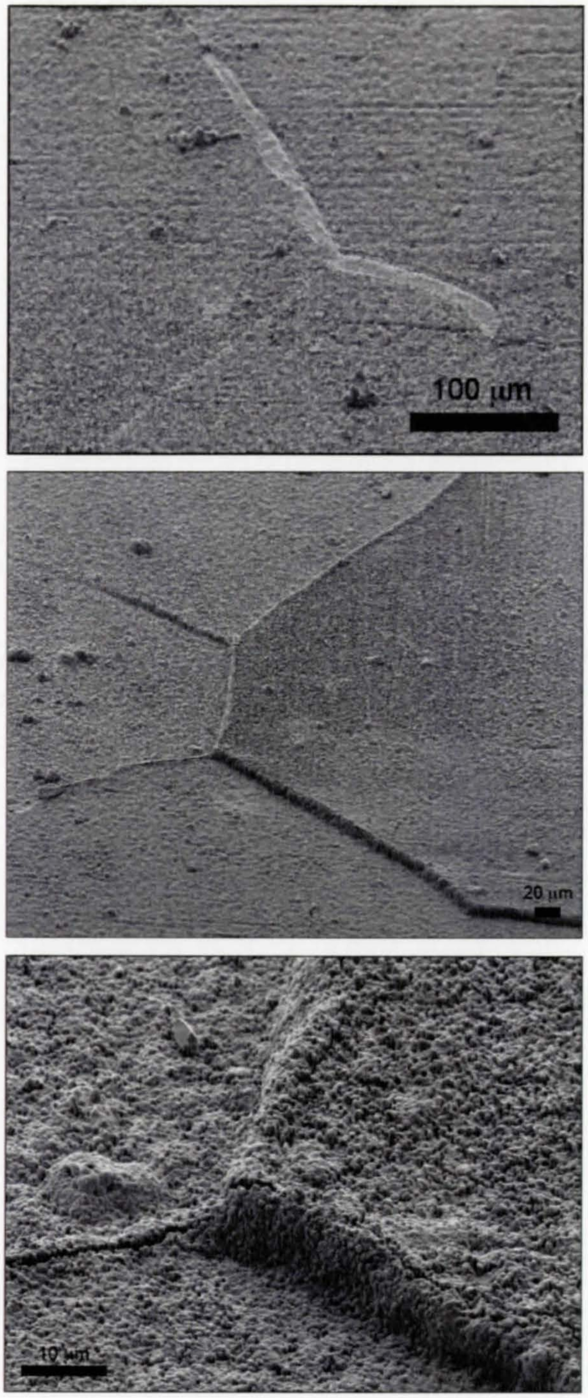

Figure B.1. Magnification of grain uplift for samples oxidized at 1200°C with 1 177 MPa for 6 hrs.

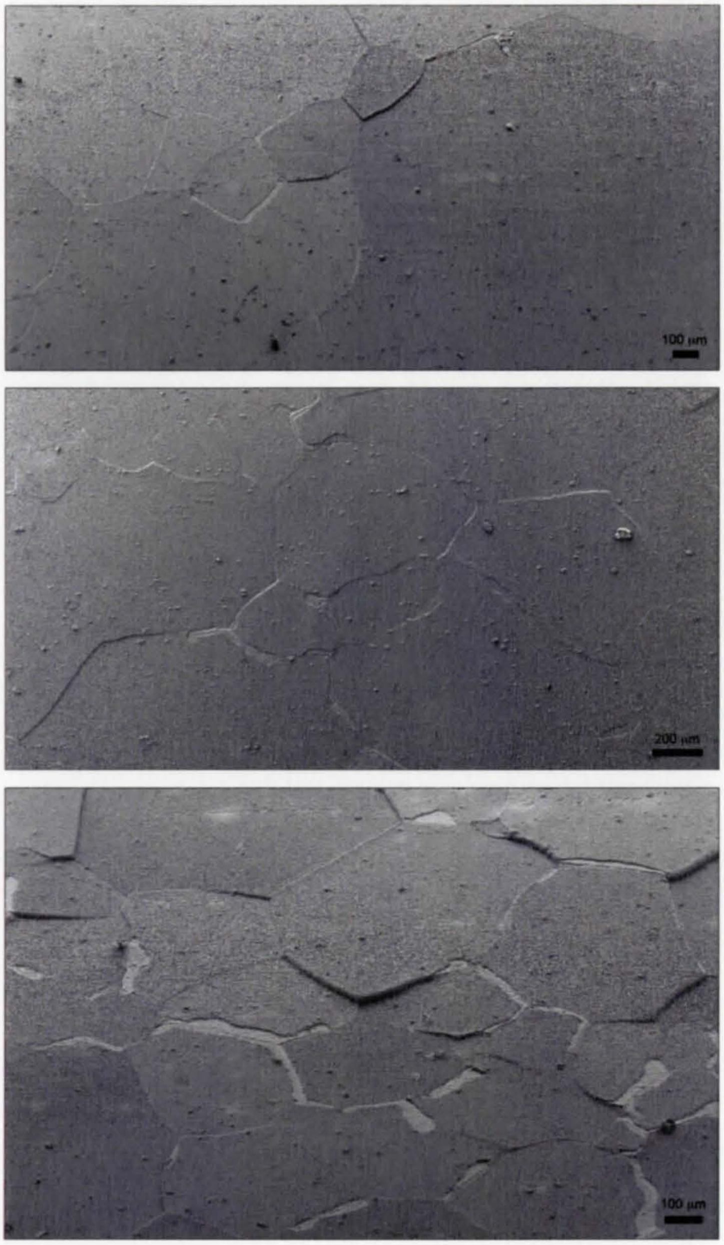

6 hrs

12 hrs

24 hrs

Figure B.2: SEM micrographs showing increase in grain uplift, cracking and spallation with respect to increasing time. Oxidation was at 1200°C with 1.177 MPa.

Similar findings for the same material has been observed by Nychka, et al. (2004) in experiments involving short wires with diameters ranging from 5 mm to 2 μm oxidized at high temperatures without applied stress (Figure B.3). These experiments demonstrated that the extent of grain uplift, cracks, and spallation in a sample was strongly dependent on the diameter of the wire. Wires with diameters greater than 2 mm showed little or no signs of uplift. Additionally, the same samples that presented with larger cracks and uplift, also showed the greater amount of plastic elongation. Based on their observations, the authors suggested that grain uplift, which leads to cracks and spallation in the oxide, was a result of grain boundary sliding in the underlying substrate during oxidation. This process was a response to compressive stresses generated during scaling. They concluded that as compressive stresses developed, the force balance will cause the underlying substrate to response with tensile stresses. If these tensile stresses exceed the flow stress at oxidizing temperatures, the substrate will plastically deform by grain boundary sliding and grain uplift in order to relax the stress.

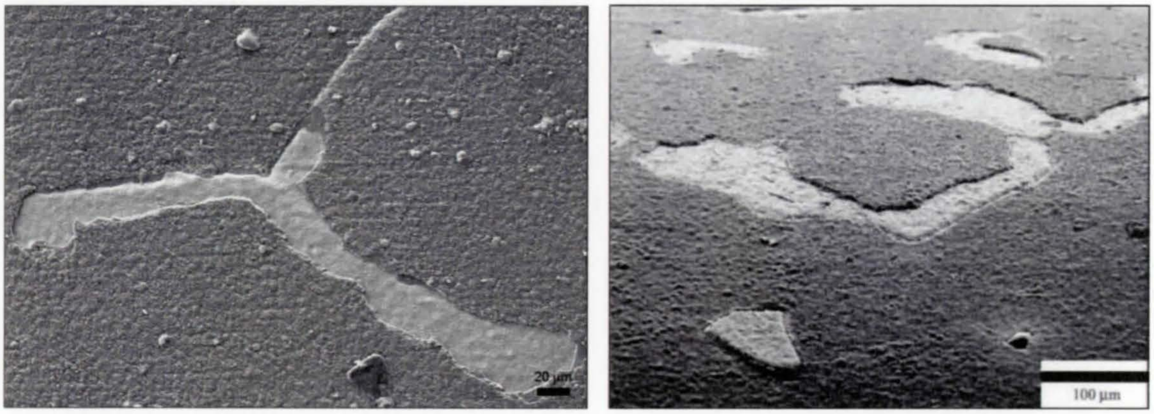

(a) (b)

Figure B.3: (a) Sample oxidized at 1200°C for 12 hrs with applied tensile load, current study. (b) Sample oxidized at 1200°C for 10 hrs with no load (Nychka et al., 2004)

Using the same argument, the observed cracks and grain uplift in the samples subjected to a tensile stress in this study is due to relaxation of compressive stresses that accompanied oxide growth. During oxidation the substrate plastically deform by grain boundary sliding in order to relax its tensile stresses, generated and applied; thus, leading to the above observations (Figure B.2, B.1)

Bibliography

Kanthal Sandvik.

JCPDS 81-1667.

Horiba Jobin Yvon, Raman Division.

Badini, C. & Laurella, F. 2001, Surface & Coatings Technology *135*(2-3), 291–298.

Berthome, G., EN'Dah, Wouters, Y., & Galerie, A. 2005, Materials and Corrosion *56*(6), 389–392.

Blachčre, J., Schumann, E., Meier, G., & Pettit, F. 2003, Scripta Materialia, 49, 909–912.

Calvarin-Amiri, G., Gourgues, A., Huntz, A., & Molins, R. 2001, Mat Sci Eng A-Struct *298*(1-2), 200–208.

Calvarin-Amiri, G., Molins, R., & Huntz, A. 2000, Oxid Met *53*(3-4), 399–426.

Carroll, D. F., Wiederhorn, S. M., & Roberts, D. E. 1989, J Am Ceram Soc *72*(9), 1610–1614.

Clarke, D. 2003, Acta Materialia, 51, 1393–1407.

Clarke, D., Tolpygo, V., & Gentleman, M. 2004, Mater Sci Forum, 461-464, 621–629.

Cueff, R., Buscail, H., Caudron, E., Issartel, C., & Riffard, F. 2003, Applied Surface Science *207*(1-4), 246–254.

Evans, H. 1995, Mat Sci Eng A-Struct *203*(1-2), 117–127.

Evans, H., Norfolk, D., & Swan, T. 1978, Journal of the Electrochemical Society *125*(7), 1180–1185.

Evans, H. E. & Lobb, R. C. 1984, Corrosion Science *24*(3), 209–222.

Jedlinski, J. 1997, Solid State Ionics, 101, 1033–1040.

Limarga, A. 2008. Personal correspondence.

Limarga, A. & Wilkinson, D. 2006, Mat Sci Eng A-Struct *415*(1-2), 94–103.

Limarga, A., Wilkinson, D., & Weatherly, G. 2004, Scripta Materialia *50*(12), 1475–1479.

Lipkin, D. M. & Clarke, D. 1996, Oxid Met *45*(3/4), 267–280.

Luecke, W. E., Wiederhorn, S. M., Hockey, B. J., Ralph F. Krause, J., & Long, G. G. 1995, J Am Ceram Soc *78*(8), 2085–2096.

Mennicke, C., Clarke, D., & Ruhle, M. 2001, Oxid Met *55*(5-6), 551–569.

Nychka, J. & Clarke, D. 2005, Oxid Met *63*(5-6), 325–352.

Nychka, J., Pullen, C., He, M., & Clarke, D. 2004, Acta Materialia *52*(5), 1097–1105.

Pilling, N. & Bedworth, R. 1923, J. Inst. Metals, 29, 529–589.

Rhines, F. & Wolf, J. 1970, Metallurgical and Materials Transactions B.

Rolls, R. & Shahhosseini, M. 1982, Oxid Met *18*(3-4), 115–126.

Stott, F. H. 1997, Mater Sci Forum, 251-254, 19–32.

Sully, A. H. 1949. *Metallic Creep and creep resistant alloys.* London Butterworths Scientific Publications.

Toesca, S., Pourantru, Y., & Colson, J. C. 1981. The effect of mechanical stress on the kinetics and mechanism of sulphidation of a fecral alloy at high temperature. In *Corrosion and mechanical stress at high temperatures*, pp. 379–388. Applied Science.

Tolpygo, V. & Clarke, D. 1998a, Oxid Met *49*(1-2), 187–212.

Tolpygo, V. & Clarke, D. 1998b, Acta Materialia *46*(14), 5153–5166.

Tolpygo, V. & Clarke, D. 1999, Surface & Coatings Technology, 120, 1–7.

Tolpygo, V. & Clarke, D. 2003, Materials at High Temperatures *20*(3), 261–271.

Tolpygo, V., Dryden, J., & Clarke, D. 1998, Acta Materialia *46*(3), 927–937.

Wilber, J., Bennett, M., & Nicholls, J. 2000, Materials at High Temperatures *17*(1), 125–132.